Theoretical Exploration of Ultrafast Spectroscopy of Small Clusters

V. BONAČIĆ-KOUTECKÝ, MICHAEL HARTMANN, JIŘÍ PITTNER,* HUUB VAN DAM†

Walther-Nernst-Institut für Physikalische und Theoretische Chemie, Humboldt-Universität zu Berlin, Bunsenstraße 1, D-10117 Berlin, Germany

Received 2 August 2000; revised 26 February 2001; accepted 12 March 2001

ABSTRACT: The central issue in femtosecond (fs) time resolved spectroscopy of clusters is the investigation of geometric relaxation and internal vibrational redistribution (IVR) after optical excitation in a nonequilibrium configuration of nuclei by laser photoelectron excitation, and corresponding time delayed probing by multiphoton-ionization. For this purpose, we have developed multistate ab initio molecular dynamics involving adiabatic ground and excited electronic states, as well as nonadiabatic coupling between them, using the time evolution of initial thermal ensemble in Wigner representation. The combination of ab initio quantum chemical methods, used for the adiabatic and nonadiabatic molecular dynamics "on the fly," and the Wigner distribution approach for the description of the motion of the nuclei allowed us the accurate determination of pump-probe and pump-dump signals also under temperature dependent initial conditions. The connection between simulated pump-probe signals and the underlying dynamics of nuclei involving adiabatic electronic ground states has been first established for the example of the $Ag_3^-/Ag_3/Ag_3^+$ systems, and compared with experimental negative-to-neutral-to-positive *NeNePo pump-probe* signals. Our simulations reproduced the experimental *NeNePo* results and determined, in addition to the timescales of geometric relaxation, the conditions under which the resonant or dissipative IVR, as well as vibrational coherence, should be found in the experimental pump-probe signals. This can be realized in the zero electron kinetic energy *NeNePo-ZEKE* experiments, which are in progress. The above combination of methods has been recently extended to the analysis of the timescales as well as of the dynamics in excited electronic states of the nonstoichiometric Na_nF_{n-1} ($n = 2$–4) clusters with the single excess valence electron. Our approach allows the simulation of femtosecond *NeExPo-pump-probe* and *NeExNe-pump-dump* signals, based on an analytic formulation which utilizes temperature

Correspondence to: V. Bonačić-Koutecký; e-mail: vbk@kirk.chemie.hu-berlin.de.

*Permanent address: J. Heyrovský Institute of Physical Chemistry, Academy of Sciences of the Czech Republic, Dolejškova 3, CZ-18223 Prague, Czech Republic.

†Permanent address: CLRC Daresbury Laboratory, Daresbury, Warrington, Cheshire, UK, WA4 4AD.

Contract grant sponsor: Deutsche Forschungsgemeinschaft.

Contract grant number: 450.

dependent ground state initial conditions of neutral system (*Ne*); an ensemble of trajectories carried out either on the adiabatic electronic excited state (*Ex*), or on both the excited and the ground states through nonadiabatic coupling in connection with the fewest switching hopping algorithm for the investigation of the dynamics of the system; and either the cationic (*Po*) or the neutral ground state (*Ne*) for the probing step. The choice of the systems has been made in order to determine the timescales of processes involving (1) fast geometric relaxation leaving the bonding frame intact versus IVR, as during the adiabatic dynamics in the first excited state of Na_4F_3, being the smallest prototype of F-colored centers in the bulk; and (2) the photo-isomerization process through the conical intersection during nonadiabatic dynamics due to the long amplitude motion, as in the Na_3F_2 cluster after breaking of one metallic and one ionic bond, representing the first example of a five atomic cluster in the gas phase exhibiting conical intersection between the ground and the first excited state. In both cases, full complexity of the problem has been considered taking into account all degrees of freedom. The investigated systems represent important test cases for providing the conceptual framework of ultrafast dynamics in finite systems. Int J Quantum Chem 84: 714–739, 2001

Key words: nonadiabatic coupling; internal vibrational redistribution; pump-probe signals

Introduction

Femtosecond spectroscopy allows for the real-time investigation of intramolecular and intermolecular electronic and nuclear dynamics during chemical transformations. The basic idea involves the preparation of a transition state of the chemical reaction by optical excitation of a stable species in a nonequilibrium nuclear configuration, and probing its time evolution by laser induced techniques (e.g., fluorescence, photoelectron spectroscopy, or multiphoton ionization). This approach was pioneered by Zewail et al. for bimolecular reactions [1–3]. Transition states can be also generated by vertical photodetachment of stable negative ions, where the ground state is characterized by a geometry close to that of the transition state of the corresponding neutral species as shown by Neumark et al. [4–6]. The vertical photodetachment can also produce transition states for intramolecular isomerization of the neutral species as shown by Lineberger et al. [7–9]. Wöste and his colleagues [10] advanced the vertical one-photon detachment technique in their negative ion-to-neutral-to-positive ion (*NeNePo*) pump-probe experiments. They were able to prepare neutral Ag_n clusters in their transient ground states by one-photon detachment of Ag_n^- and to investigate the time evolution of the neutral species by a delayed ionizing pulse via two-photon ionization. An extension of the *NeNePo* experimental technique by Lineberger et al. [11] using two-color excitation confirmed important aspects of this approach.

However, the theory and the simulations provide the conceptual framework of the ultrafast dynamics by determining the timescales and the nature of the configurational changes and internal vibrational energy redistributions in vertically excited or ionized states of molecules and clusters [12–15]. In this context, clusters are of particular interest since their dynamical properties can be studied as a function of their size or of their degrees of freedom, and therefore a transition between resonant and dissipative features of finite systems might become accessible. The nuclear dynamics of clusters allows for the separation of timescales of intracluster and intercluster motions [16, 17].

In this article, we wish to show that the accurate simulation of the femtosecond time resolved pump-probe and pump-dump signals allows for the identification of different processes such as geometric changes of different types and intramolecular vibrational relaxation (IVR) of different nature, as well as for determination of their timescales. For this purpose, we (1) developed an ab initio molecular dynamics for ground [18] and excited [19–21] states including nonadiabatic coupling "on the fly," (2) employed it in the context of a multistate nuclear dynamics for the generation of the initial conditions, for the system itself and for the probe or dump step, and (3) combined it with the Wigner distribution approach to nuclear dynamics which allowed to simulate fs signals from analytically derived expressions [14, 15, 19–21].

We have chosen to present three types of examples. (1) The results of the simulations of the pump-probe signals for $Ag_3^-/Ag_3/Ag_3^+$ which in-

volve multistate dynamics on the corresponding ground states since the experimental *NeNePo* signals are available for comparison, this system also served as a test for our newly developed ab initio Wigner distribution approach [14]. (2) The results of the pump-dump signals for Na_4F_3 cluster because the multistate dynamics involve not only ground but also the first excited electronic state, and also because for a system of this size the precalculation of the adiabatic energy surfaces for all degrees of freedom is not feasible [20]. (3) The results of the pump-probe signals of Na_3F_2 cluster because of nonadiabatic dynamics through conical intersection are a consequence of radiationless decay of the first excited state [21]. This means that the nuclear motion occurs on two potential energy surfaces despite the fact that the process begins and ends on the ground state potential-energy surface. This circumstance, together with the fact that we have to deal with large vibrational excess energy, simplifies the situation allowing us to avoid the consideration of the geometric phase effect around the conical intersection, which is the subject of numerous investigations based on fully quantum mechanical dynamics (cf. Ref. [22] and references therein). Moreover, since we consider it necessary to take into account all degrees of freedom for the nonadiabatic dynamics, the choice of the treatment is limited either to surface hopping methods or to classical-path methods characterized by problems arising from the approximation that trajectories propagate in state-specific or mean potential, respectively (cf. Ref. [23] and references therein). Due to the conical intersection passage arising from a long amplitude motion, we decided to use the fewest-switches surface hopping approach introduced by Tully [24], which has been based on the assumption that the fraction of trajectories on each surface is equivalent to the corresponding average quantum probability determined by coherent propagation of quantum amplitudes, although we are aware that this internal consistency is not always maintained [25].

In fact, the investigation of the nonadiabatic dynamics at the conical intersection of Na_3F_2 offers a unique opportunity to simulate fs pump-dump signals in the framework of the combination of the Wigner–Moyal representation of the vibronic density matrix [26] and an ab initio multistate molecular dynamics in ground and excited states without the precalculation of energy surfaces including the computation of the non-adiabatic couplings "on the fly." At the same time, it allows for the prediction and verification of consequences of conical intersections in fs pump-probe signals in the gas phase without the necessity to consider the environment which complicates the issue as in the case of photochemistry in solution or in the case of the cis-trans photo-isomerization of the visual pigment due to the influence of the protein cavity.

Moreover, for all three examples, the analysis of the simulated signals accounts for geometric relaxation as well as internal vibrational relaxation both being of different nature. In addition, all presented examples are of interest in the context of the investigation of their dynamical behavior on the fs timescale as a function of their size. The theoretical and experimental investigation of the *NeNePo* fs spectroscopy on silver clusters larger than trimers, as well as of pump-probe (*NeExPo*) and pump-dump (*NeExNe*) signals of nonstoichiometric sodium fluoride series Na_nF_{n-1}, is in progress. Both series of purely metallic clusters and ionic systems with single excess electron offer a large diversity of physical and chemical processes to be studied.

Methodology

Our ab initio Wigner distribution approach combines the Wigner–Moyal representation of the vibronic density matrix with the ab initio molecular dynamics "on the fly" in ground and/or excited electronic states under the presence of external optical fields. In particular, this method allows us to handle femtosecond multistate dynamics in order to simulate pump-probe and pump-dump signals of the ultrafast optical spectroscopy of molecular systems. It is applicable to systems of moderate size where all degrees of freedom have to be treated equaly. In the following, we give a brief outline of this method.

We begin with the exact quantum mechanical Liouville equation for the vibronic density matrix $\hat{\varrho}_{ab}(\mathbf{q},\mathbf{q}') = \psi_a(\mathbf{q})\psi_b^*(\mathbf{q}')$, where $\psi_a(\mathbf{q})$ ($\psi_b^*(\mathbf{q}')$) describes the nuclear wavefunction labeled by the electronic state a (b), and $\mathbf{q}$ ($\mathbf{q}'$) denotes the whole of the nuclear coordinates:

$$i\hbar\frac{\partial\hat{\varrho}_{ab}}{\partial t} = \hat{h}_a\hat{\varrho}_{ab} - \hat{\varrho}_{ab}\hat{h}_b - E(t)\sum_c(\hat{\mu}_{ac}\hat{\varrho}_{cb} - \hat{\varrho}_{ac}\hat{\mu}_{cb}). \quad (1)$$

The first two terms on the right-hand side are responsible for the multistate nuclear dynamics determined by the vibrational Hamiltonians $\hat{h}_a$ and $\hat{h}_b$, respectively, initiated by the field $E(t)$. The last term on the right-hand side of Eq. (1) describes the coupling of the molecular system to the field where μ

is the electronic transition dipole moment in Condon approximation. Although the system is determined by pure states, the Liouville equation offers a convenient starting point for approximate methods such as semiclassical approaches. Introducing classical phase space variables $(\mathbf{q}, \mathbf{p})$ and performing a Wigner–Moyal expansion of Eq. (1) in powers of $\hbar$ [26], equations of motion for the Wigner distributions $P_{ab}(\mathbf{q}, \mathbf{p})$ being the classical analog of the vibronic density matrix can be obtained. In lowest order with respect to $\hbar$, one obtains for the occupation density P_{aa} [14] the equation

$$i\hbar\frac{\partial P_{aa}^{(i)}}{\partial t} = \frac{\hbar}{i}\left\{\frac{\partial h_a}{\partial \mathbf{q}}\frac{\partial P_{aa}^{(i)}}{\partial \mathbf{p}} - \frac{\partial h_a}{\partial \mathbf{p}}\frac{\partial P_{aa}^{(i)}}{\partial \mathbf{q}}\right\} - E(t)\sum_c\left(\mu_{ac}P_{ca}^{(i-1)} - P_{ac}^{(i-1)}\mu_{ca}\right), \quad (2)$$

and for the transition probabilities P_{ab}

$$i\hbar\frac{\partial P_{ab}^{(i)}}{\partial t} = (h_a - h_b)P_{ab}^{(i)} - E(t)\sum_c\left(\mu_{ac}P_{cb}^{(i-1)} - P_{ac}^{(i-1)}\mu_{cb}\right), \quad a \neq b. \quad (3)$$

In Eqs. (2) and (3), we additionally performed an expansion of the Wigner distributions with respect to the field $E(t)$, giving rise to the superscript (i) labeling the order in the field. Thus we restrict ourselves to low field intensities, which is well justified for the calculation of pump-probe or pump-dump signals involving the transitions between electronic states. Eq. (3) can be straightforwardly integrated yielding Franck–Condon-type coupled dynamics on the electronic states during the presence of the field, including the transition between the states. Eq. (2) describing the dynamics upon an electronic state after the excitation can be solved by integrating Hamilton's equations, e.g., for the state a it is $\dot{\mathbf{q}}_a = \partial h_a/\partial \mathbf{p}_a$, $\dot{\mathbf{p}}_a = -\partial h_a/\partial \mathbf{q}_a$, which determines classical trajectories on the electronic states. For this, an ensemble of initial conditions have to be assumed, which in the case of the simulation of pump-probe or pump-dump signals can be naturally determined from the vibronic Wigner distribution of the initial electronic state, i.e., before any field is present. We assume a thermal distribution for the initial ensemble in order to be able to include temperature effects in correspondence with the experimental situations. For higher temperature of the initial ensemble (some hundreds of K), the initial conditions are generated by sampling a long-time trajectory upon the initial electronic state with constant averaged kinetic energy or constant total energy corresponding to a canonical or microcanonical ensemble, respectively. This allows us to include anharmonicities and vibrational couplings of the initially prepared molecular system at higher temperatures. For low temperatures, quantum effects of the initial ensemble have to be taken into account and, therefore, we used the expression for the Wigner distribution of a canonical ensemble in each of the normal modes. Initial conditions are then obtained by sampling this distribution function.

Based on the classical trajectories and assuming Gaussian femtosecond envelopes for the laser fields, an analytical expression for the time resolved *NeNePo-ZEKE* pump-probe, *NeExNe* pump-dump, and *NeExPo* signals including crossing through conical intersection can be derived, respectively [14, 20, 21].

$$\begin{aligned} S[t_d]^{NeNePo\text{–}ZEKE} &\sim \int d\mathbf{q}_0\, d\mathbf{p}_0 \int_0^\infty d\tau_1 \exp\left\{-\frac{(\tau_1 - t_d)^2}{\sigma_{pu}^2 + \sigma_{pr}^2}\right\} \\ &\times \exp\left\{-\frac{\sigma_{pr}^2}{\hbar^2}\left[E_{pr} - V_{+1,0}\left(\mathbf{q}_1(\tau_1; \mathbf{q}_0, \mathbf{p}_0)\right)\right]^2\right\} \\ &\times \exp\left\{-\frac{\sigma_{pu}^2}{\hbar^2}\left[E_{pu} - V_{0,-1}(\mathbf{q}_0)\right]^2\right\} P_{-1,-1}^{(0)}(\mathbf{q}_0, \mathbf{p}_0), \end{aligned} \quad (4)$$

$$\begin{aligned} S[t_d]^{NeExNe} &\sim \int d\mathbf{q}_0\, d\mathbf{p}_0 \int_0^\infty d\tau_1 \exp\left\{-\frac{(\tau_1 - t_d)^2}{\sigma_{pu}^2 + \sigma_{du}^2}\right\} \\ &\times \exp\left\{-\frac{\sigma_{du}^2}{\hbar^2}\left[E_{du} - V_{+1,1}\left(\mathbf{q}_1(\tau_1; \mathbf{q}_0, \mathbf{p}_0)\right)\right]^2\right\} \\ &\times \exp\left\{-\frac{\sigma_{pu}^2}{\hbar^2}\left[E_{pu} - V_{10}(\mathbf{q}_0)\right]^2\right\} P_{00}^{(0)}(\mathbf{q}_0, \mathbf{p}_0), \end{aligned} \quad (5)$$

$$\begin{aligned} S[t_d]^{NeExPo} &\sim \int d\mathbf{q}_0\, d\mathbf{p}_0 \int_0^\infty d\tau_1 \exp\left\{-\frac{(\tau_1 - t_d)^2}{\sigma_{pu}^2 + \sigma_{pr}^2}\right\} \\ &\times \frac{1}{N_{hop}}\sum_\nu \exp\left\{-\frac{\sigma_{pr}^2}{\hbar^2} \times \left[E_{pr} - V_{+1,x}\left(\mathbf{q}_x^\nu(\tau_1; \mathbf{q}_0, \mathbf{p}_0)\right)\right]^2\right\} \\ &\times \exp\left\{-\frac{\sigma_{pu}^2}{\hbar^2}\left[E_{pu} - V_{10}(\mathbf{q}_0)\right]^2\right\} P_{00}^{(0)}(\mathbf{q}_0, \mathbf{p}_0). \end{aligned} \quad (6)$$

Pump-probe time resolved signals for the negative ion-to-neutral-to-positive ion process (*NeNePo*) obtained by photodetachment and photoionization

are proportional to the Wigner density of the cation, $P_{+1,+1}(\mathbf{q}, \mathbf{p})$, and require a classical trajectory calculation on the adiabatic ground state of the neutral species. Pump-dump or pump-probe signals between the ground and excited states (*NeExNe* or *NeExPo*) are proportional to the field induced Wigner density of the ground state $P_{00}(\mathbf{q}, \mathbf{p})$, and require either a classical trajectory calculation on the adiabatic excited state or, in the case of the nonadiabatic dynamics, the propagation of the ensemble starts at the excited state but may hop at the ground state according to the fewest-switching hopping algorithm. In the latter case, not only is the common averaging over the whole ensemble of the initial conditions due to the Wigner approach required, but also, for a given initial condition, an averaging over trajectories obtained from different random numbers according to the hopping algorithm has to be carried out. Therefore, we denote the coordinates and momenta of the propagated state by $\mathbf{q}_x^\nu$ and $\mathbf{p}_x^\nu$, where x is either the excited or the ground state which is determined by the hopping procedure. The ν numerates the set of random numbers used in the hopping algorithm obeying the same initial condition. Consequently, we have to average over the number of hoppings N_{hop}. According to Eq. (6), the initial ground state density $P_{00}^{(0)}(\mathbf{q}_0, \mathbf{p}_0)$ is promoted to the first excited state with the Franck–Condon transition probability given by the last exponential of Eq. (6). The propagation, the passing of the conical intersection, and the probe transition to the cationic state are described by the second exponential. The probe pulse window being located around the time delay t_d between the pump and the probe pulse and the resolution of the signal determined by the square of the pulse durations is given by the first exponential. As is required in the Wigner distribution approach, an ensemble average over the initial conditions has to be performed. The latter can be obtained from a sampling of the initial vibronic Wigner distribution $P_{00}^{(0)}$ of the ground electronic state. In the case of pump-dump signals, probing in the gas phase corresponds to a transition of the dumped ground state density to the cation.

As input for the simulation of the signals, the calculations of the trajectories "on the fly" have to be carried out. This involves the computation of the forces with quantum chemical gradient based methods originally developed for geometry optimization. This is much simpler for ground states than for excited states. We use our ab initio molecular dynamics with Gaussian atomic basis based on gradient corrected density functional [18] for the dynamics involving ground states for *NeNePo* spectroscopy of $Ag_n^-/Ag_n/Ag_n^+$. Of course, for trimers even more sophisticated methods such as CCSD can be used, or the energy surfaces can be precalculated [14].

The excited state ab initio dynamics require for the calculation of the forces a more complicated electronic response with respect to the nuclear displacements. Here we present a particularly simple case for the nonstoichiometric sodium fluorides with a single excess electron [27, 28]. In these systems, the $n - 1$ valence electrons of the alkali atoms are almost "localized " at the fluorine atoms, forming strongly polar, nearly ionic bonds which are not influenced by processes involving the single excess electron. It is therefore to be expected that only the excess electron is responsible for the absorption patterns of these systems, particularly in the low transition energy region with dominant intensity (in which the stoichiometric clusters do not give rise to any intense transition). This has been confirmed by comparing the results obtained from MRCI [27, 28] in which excitations of all valence electrons were allowed. The very special character of these systems has been also recognized by Ahlrichs et al. [29] who used the unrestricted Hartree–Fock random phase approximation (UHF-RPA) for the computation of the absorption spectra of the nonstoichiometric ionically bonded alkali halide clusters. However, we have introduced an even more simplified treatment in the framework of the "frozen ionic bond" approximation [28] which has the following advantages. It allows the accurate computation of the absorption spectra of the systems with one-electron excess at low computational demand; it avoids the spin contamination problem being inherently present in the UHF based methods; and mainly it permits fast calculations of analytic gradients in excited states as well as of nonadiabatic couplings between adiabatic states [20, 21]. The two latter aspects are particularly important in the context of the multistate fs dynamics. In fact, the analytic gradients for the geometry optimization of the excited states in the framework of the RPA method recently became available [30, 31], allowing us to carry out MD in the excited states at low computational demand, but the analytic expressions for the calculation of the nonadiabatic coupling have not yet been derived.

In the "frozen ionic bond" approximation, the transition density matrices in the MO basis (and

subsequently the absorption spectrum) can be obtained from an effective one-excess electron Hamiltonian containing Coulomb and exchange operators with core (cf. Appendix A and Ref. [28]). Furthermore, for the dynamics in excited states, we need the gradients of the energy expression involving the gradients of the Coulomb energy of the nuclei, and of the HF energy, which are both well known [32], as well as the gradients of the energies of the excess electrons $\nabla_R \epsilon_i$ (cf. Appendix A and Refs. [19, 20]). The gradients also involve the derivatives of the one- and two-electron integrals as well as the response of the MO coefficients $C_{\alpha i}$ with respect to the nuclear displacements

$$\nabla_R C_{\alpha i} = \sum_{j=1}^{M} C_{\alpha j} U_{ji}^R \tag{7}$$

where, in general, the U matrices contain elements for which the corresponding orbital transformations either change the Hartree–Fock energy or only canonicalize the MOs. Since the MO coefficients in our approach are those of the restricted open shell Hartree–Fock (ROHF), the U matrices have to be obtained from the solution of the coupled perturbed Hartree–Fock equations (CPHF) for the open shell RHF (cf. Ref. [33]). Usually in quantum chemistry, the CPHF equations are needed as an intermediate step for the analytic computation of the vibrational frequencies. Obviously, only those U matrix elements are required for which the corresponding orbital transformations do change the HF energy. For our purpose, however, the calculation of the derivatives of ϵ_i requires the knowledge of all U matrix elements, including those corresponding to the canonicalization of the MOs [34] (cf. Appendix A). Therefore, we used the formulation and efficient implementation of the *extended* CPHF equations due to Rice et al. [35] and Lee et al. [36] which yields all U matrix elements as a solution of a system of linear equations.

Moreover, the use of the extended CPHF equations allows for the straightforward analytic formulation of nonadiabatic coupling $\langle \psi_j | \nabla_R | \psi_i \rangle$ as outlined in Appendix B and Ref. [21]. Therefore, both adiabatic and nonadiabatic dynamics can be carried out "on the fly" at low computational demand in the framework of the "frozen ionic bond" approximation.

In the latter case, we need connection between the analytic formulation of the first order nonadiabatic couplings and the MDQT based on Tully's stochastic fewest-switches procedure [24], which requires a simultaneous solving of the time dependent Schrödinger equation for the one-excess electron and classical equations of motion for the nuclei. The time dependent wavefunction $\Psi(t, r, R)$ which describes the electronic state at the time t is expanded in terms of the adiabatic electronic basis functions ψ_j of the one-electron excess effective Hamiltonian with complex-valued time dependent coefficients

$$\Psi(t, \boldsymbol{r}, \boldsymbol{R}) = \sum_{j=o}^{M} c_j(t) \psi_j(\boldsymbol{r}; \boldsymbol{R}). \tag{8}$$

The adiabatic states are also time dependent through the classical trajectory $R(t)$. Substitution of this expansion into the time dependent Schrödinger equation, multiplication by ψ_k from the left, and integration over $\boldsymbol{r}$ yields a set of linear differential equations of the first order for the expansion coefficients which are equations of motion for the quantum amplitudes:

$$\mathrm{i}\dot{c}_k(t) = \sum_j \left[\epsilon_j \delta_{kj} - \mathrm{i}\dot{\boldsymbol{R}}(t) \cdot \langle \psi_k | \nabla_R | \psi_j \rangle \right] c_j(t), \tag{9}$$

where the ϵ_j are the eigenvalues of the effective Hamiltonian, and the expression for nonadiabatic couplings $\langle \psi_k | \nabla_R | \psi_j \rangle$ has been derived in Appendix B.

The system of Eq. (9) has to be solved simultaneously with the classical equations of motion for the nuclei

$$M\ddot{\boldsymbol{R}} = -\nabla_R E_m(\boldsymbol{R}), \tag{10}$$

where the force is the negative gradient of the potential energy of the "current" mth adiabatic state

$$\nabla_R E_m(\boldsymbol{R}) = \nabla_R E^{HF}(\boldsymbol{R}) - \nabla_R \epsilon_o(\boldsymbol{R}) + \nabla_R \epsilon_m(\boldsymbol{R}), \tag{11}$$

and hopping probabilities g_{ij} between the states are determined by

$$g_{ij} = 2\frac{\Delta t}{c_i c_i^*} \left[\Im(c_i^* c_j \varepsilon_i \delta_{ij}) - \Re\left(c_i^* c_j \dot{\mathbf{R}} \langle \psi_i | \nabla_R | \psi_j \rangle \right) \right] \tag{12}$$

and can occur randomly according to the fewest-switches surface hopping approach introduced by Tully [24]. The gradients $\nabla_R \epsilon_m(\boldsymbol{R})$ in Eq. (11) have been outlined in Appendix A in connection with adiabatic dynamics. Eqs. (10) and (11) for the propagation of the coordinates and momenta are numer-

ically solved by using the velocity-Verlet algorithm where, as for the integration of Eq. (9), the Bulirsch–Stoer predictor-corrector method with variably adjusted time step has been employed. In such a way, the molecular dynamics simulations "on the fly" for Na_3F_2 were carried out with an energy conservation better than 10^{-4} eV.

We derived all analytic expressions needed to carry out the nonadiabatic MDQT "on the fly" using the fewest-switches hopping algorithm by Tully [24] which has been designed to satisfy the statistical distribution of state populations at each time according to the quantum probilities $|c_i|^2$ using a minimal number of "hops" necessary to achieve this condition (for details, cf. Ref. [24]). However, this internal consistency is not always maintained as shown in Ref. [25]. Therefore, we draw the conclusion that in order to obtain the time evolution of the population, the fraction of trajectories is more reliable than the averaged quantum probabilities, and sufficient accuracy can be expected. Thus we employed the fraction of trajectories for the simulation of the pump-probe signals presented later.

In summary, the calculation of the electronic energies in the "frozen ionic bond" approximation and the solution of Hamilton's equation of motion for the nuclei, together with the solution of the extended CPHF equations, allow the simulation of the adiabatic molecular dynamics in an electronically excited state, as well as of nonadiabatic dynamics involving the propagation in the excited state and in the ground state after the passage through the conical intersection in the framework of the above-described model. This classical treatment of nuclei is applicable to problems where quantum interference effects are washed out, which is usually the case, e.g., at high temperatures. In particular, quantum coherence and tunneling are excluded. In more sophisticated approaches, e.g., in the semiclassical initial value representation (SC-IVR), these effects can be taken into account [37]. Other semiclassical formulations are the semiclassical multiple surface hopping propagator approach [38], the multiple spawning method [39], the quantum-classical density matrix approach involving a hybrid MD–Monte-Carlo algorithm with momentum jumps [40], and the semiclassical multistate Liouville dynamics in diabatic [41] and adiabatic representation [42]. These methods are computationally more demanding and are usually applied on model systems.

Simulation of Pump-Probe Signals for $Ag_3^-/Ag_3/Ag_3^+$ and Interpretation of NeNePo Experiments

In this experiment, a transient linear Ag_3 cluster in its ground electronic state was prepared by one-photon detachment of the linear Ag_3^-, and its temporal evolution from the linear to the triangular Ag_3 structure was investigated by a delayed ionizing pulse via two-photon ionization. Figure 1 shows the scheme of the multistate fs dynamics and the energy gaps for $Ag_3^-/Ag_3/Ag_3^+$ in the Franck–Condon regime, as well as in the minimum of the neutral Ag_3 which will be used for determining the excitation energies of the pump E_{pu} ($2.95\ \text{eV} \leq E_{pu} \leq 3.13\ \text{eV}$) consisting of the vertical detachment VDE = 2.45 eV and the continuum, and for the probe E_{pr} ($6.67\ \text{eV} \geq E_{pr} \geq 5.73\ \text{eV}$) ranging from the vertical ionization potential of the linear geometry VIP_{lin} to the VIP of the triangular species. Notice that for trimers we precalculated the ground state energies of Ag_3^-, Ag_3, and Ag_3^+ at the correlated level of theory (cf. Ref. [14]). For initiating the simulation, initial conditions were prepared for an ensemble of 1000 coordinates and momenta sampled at time intervals of 10 fs from a microcanonical trajectory of 10 ps obtained from MD of the anion. Equilibration was achieved by rescaling

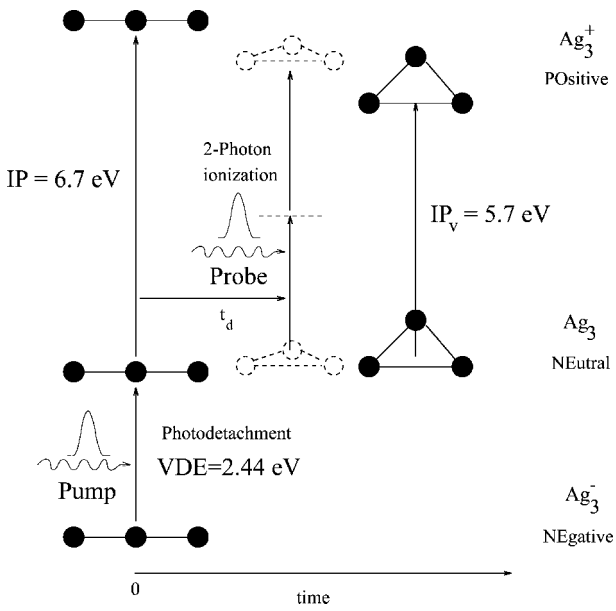

FIGURE 1. Scheme of the multistate fs dynamics on Ag_3.

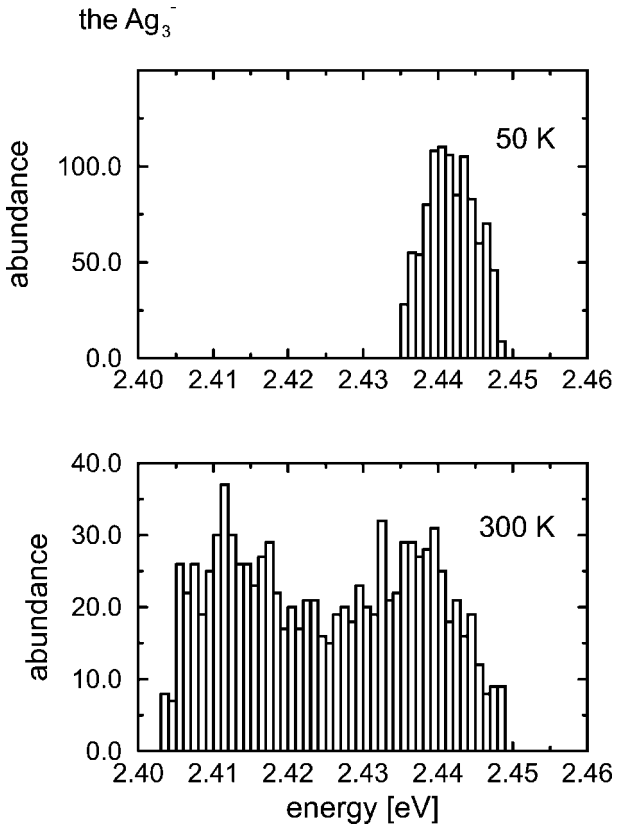

FIGURE 2. Histograms of the vertical detachment energies (VDE) of the Ag_3^- for 50 K and 300 K, respectively.

the velocities until the time averaged E_{kin} was in correspondence with the derived temperature of, e.g., $T = 50$ K or 300 K.

The ensemble of the initial conditions for the dynamics of the Ag_3 are characterized by the Franck–Condon transition probabilities in terms of the abundances of the VDE's between the Ag_3 and the Ag_3^- (Fig. 2). The maximum of the VDE at 2.45 eV corresponds to the linear geometry of the anion, and therefore represents an upper limit which is temperature independent. The asymmetric line broadening for the 300 K ensemble stems from the energy difference of Ag_3^- and Ag_3 along the bending mode. Using the ensembles with 50 K and 300 K initial temperatures, we first simulated *NeNePo-ZEKE* signals with zero pump-pulse durations ($\sigma_{pu} = 0$), which means that the entire anionic initial ensemble prepared at the given temperature is excited by the pump. In Figure 3 we present the simulated *NeNePo-ZEKE* signals for the ensemble with 50 K and 300 K initial temperature for three different excitation energies and for Gaussian probe pulse duration of 100 fs corresponding to experimental conditions. $E_{pr} = 6.5$ eV is close to the initial Franck–Condon transition, while $E_{pr} = 5.8$ eV corresponds to the probing of the minimum of the neutral (Jahn–Teller region) and $E_{pr} = 6.1$ eV has an intermediate energy. The first two energies have been chosen for the investigation of the geometrical changes versus IVR, respectively. In order to illustrate the nature of IVR, bunches of trajectories of the 50 K and the 300 K ensemble projected on a Q_x (bending mode), Q_s (symmetric stretch mode) contour plot of the cation-neutral energy gap surface are also shown in Figure 3.

For the simulated signals at low temperature and for $E_{pr} = 6.5$ eV close to the Franck–Condon region, the signal appears after 450 fs and reaches the maximum at 700 fs, reflecting the changes of the vertical ionization energies due to the geometrical change from the linear to the triangular geometry prior the onset of IVR for $E_{pr} = 5.8$ eV close to the Jahn–Teller region. After geometry relaxation has been completed, at the closest approach of the terminal atoms (Jahn–Teller region), a strong repulsion takes place which we call intracluster collision. It induces a sudden energy transfer from the bending to the symmetric stretching mode. The time σ_{coll}^{ON} for the onset of the collision (950 fs) almost coincides with the onset of the IVR. The pronounced broad peak with high signal intensity (for $T = 50$ K) can be rationalized by the bunches of the trajectories on the contour plots of the Ag_3^+–Ag_3 energy gap hypersurface in the lower part of Figure 3. After the intracluster collision at $T = 50$ K, the concerted character of the nuclear motion is preserved between 900 and 1100 fs, with the system moving along the 5.8 eV contour line with almost constant IP. For the intermediate energy $E_{pr} = 6.1$ eV, the signal has lower intensity due to the larger spread of the phase space density at longer times. In comparison with the low temperature simulation, for $T = 300$ K, the onset of the signals occurs earlier by about 200 fs due to the higher initial kinetic energy of the bending mode reflecting faster geometry relaxation. Moreover, in the IVR time domain, the $T = 300$ K ensemble exhibits spatial spread after the intracluster collision resulting in lower signal intensity than for the $T = 50$ K ensemble, since in the former case both bending and stretching modes are simultaneously excited (oscillations of the energy gaps are present). At longer times (after 2.4 ps at $T = 50$ K and 1.8 ps at $T = 300$ K), dissipative IVR results in vibrational equilibration. In summary, Figure 3 reveals that geometric

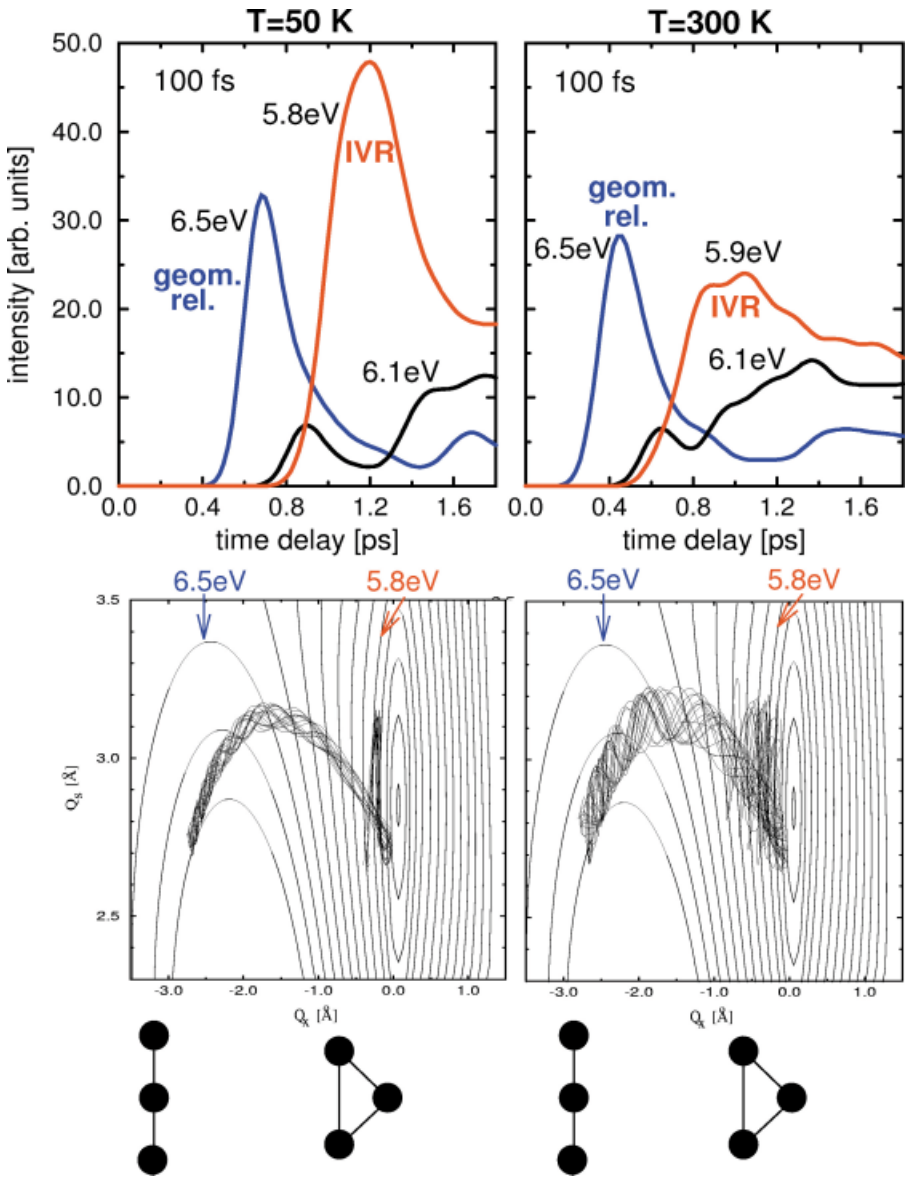

FIGURE 3. *NeNePo-ZEKE* probe signals (above) and bunches of 30 trajectories projected on the Q_xQ_s contour plot of the cation-neutral energy gap surface (below) for two different temperatures (left column, 50 K; right column, 300 K).

relaxation and IVR in Ag_3 can take place on different timescales being probed by the appropriate probe energies, and it shows that these timescales can be changed by the temperature of the initial ensemble.

Now we will turn our attention to the experimental *NeNePo* conditions for which we have included the continuum of energy for the detached electron and for the probed cation. We show on Figure 4 the comparison of the simulated and recorded *NeNePo* experiment for the 300 K initial ensemble. The clear distinction between the geometrical relaxation and IVR revealed in the *NeNePo-ZEKE* signals is no longer present. The simulated signals are in good agreement with the experimental signals obtained by Wöste et al., reflecting the fact that the experimental conditions do not allow us to distinguish individual processes such as geometric relaxation and IVR. These findings stimulated new experiments in which the temperature of the initial conditions has been varied and the corresponding timescales for the geometrical relaxation have been obtained. Fur-

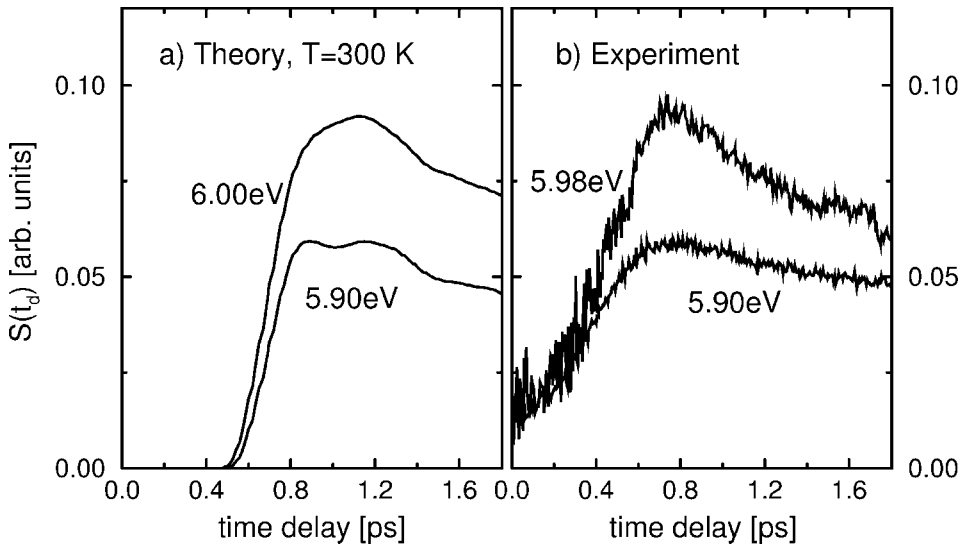

FIGURE 4. Comparison between simulated and experimental *NeNePo* signals of Ag_3. The energies labeled refer to the excitation energies of the probe.

thermore, additional experiments close to *NeNePo-ZEKE* conditions are in progress.

Simulation of the Pump-Dump Signals Illustrated on the Example of Na_4F_3 Clusters

In order to study pump-dump time resolved signals for the ground-to-excited-to-ground state of the neutral species (*NeExPo*) using the ab initio Wigner distribution approach described above, let us first address the nature of the optical response of the Na_4F_3 cluster. The optical absorption spectrum for the stable structure of Na_4F_3, which is the three-dimensional "cuboidal" structure where the corner defect represents the prototype of the "surface F-center" in finite systems [27, 28], is shown in Figure 5. The single dominant transition to the 1^2E state with a large value of the oscillator strength ($f_e = 0.62$) is located in the infrared region at 1.4 eV. This is due to the fact that the single excess electron is located in the large gap between the occupied and unoccupied one-electron functions (corresponding to the "valence" and "conductivity" bands in infinite systems) and is well separated from the MO's involved in the ionic bonding justifying the "frozen ionic bonds" approximation. Therefore, the optical response properties compare well with those calculated taking into account all valence electrons in our previous work. We use the effective core potentials and the basis sets from Ref. [27]. For the dynamics an even smaller basis set has been employed, since it provides the accurate description of the first excited state at lower computational cost.

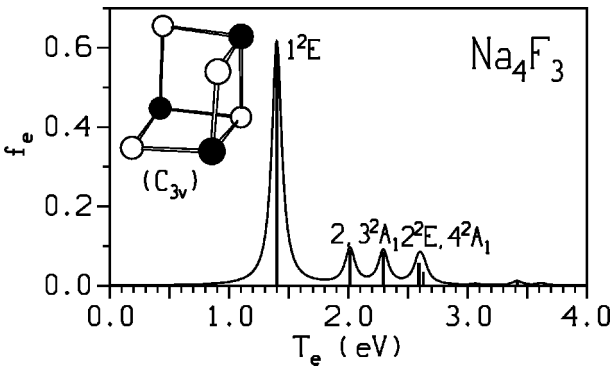

FIGURE 5. Optically allowed transitions T_e in eV and oscillator strengths f_e for the stable structure of Na_4F_3 obtained from the one-electron "frozen ionic bond" approximation.

This convenient situation allowed us to investigate the dynamics of the first adiabatic excited state as outlined in the second section and Appendix A, and to determine the timescales of the geometrical relaxation and of the IVR for the optical excitation of the single excess electron localized at the corner defect of the cuboidal structure. The pump-probe and pump-dump scheme is presented in Figure 6, with energies and structures of the minima in the

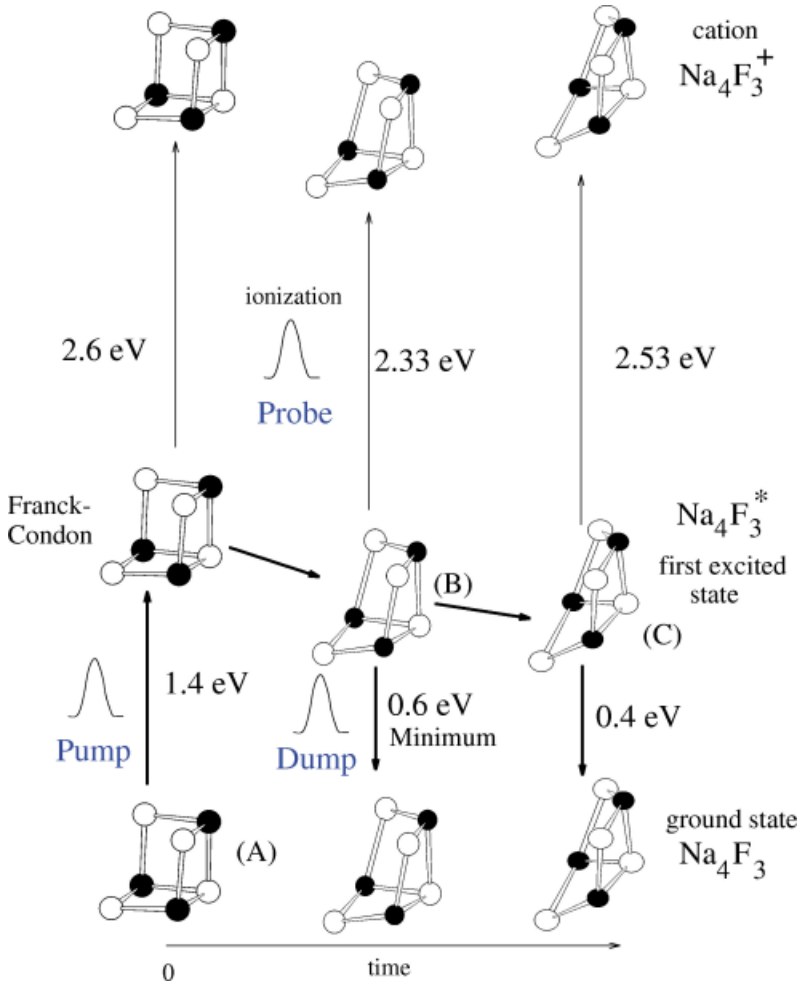

FIGURE 6. Pump-probe and pump-dump scheme of Na_4F_3 to monitor the dynamics upon the first excited state. The energies refer to the energy gaps of the pump, the dump, and the probe step at a given time, where the corresponding geometry is assumed during the dynamics.

ground (A) and the first excited (B) state. The structure of the minimum in the excited state is the strongly deformed "cage" of the cuboidal structure. The energy lowering from the vertical transition (at 1.4 eV) to the minimum of the excited state is 0.8 eV. At this point, the energy gap between the ground and the excited state is 0.6 eV. This energy gap slightly decreases for even more deformed structure (C).

The Franck–Condon profile corresponding to the abundance of the energy gaps between the first excited and the ground state for a 30 K initial ensemble is shown in Figure 7. One can detect the largest abundance close to the vertical transition (≈1.4 eV). This ensemble serves as an initial condition for the investigation of the dynamics in the first excited state. For the characterization of the ensemble dynamics, it is instructive to plot the bunches of energy gaps between the first excited state and the ground state (cf. Figure 8) since these quantities enter into the expression for the pump-dump signal. Regular cage oscillations can be monitored and are reflected in the periodical change of the gaps. However, for times beyond 1 ps, the periodicity is distorted due to the energy redistribution in other modes. This becomes clearly evident in the simulated pump-dump signals (*NeExNe*) shown in Figure 9. The simulations have been carried out for three different dump laser energies: (1) $E_{du} = 1.2$ eV is close to the Franck–Condon region; (2) $E_{du} = 0.6$ eV corresponds to the

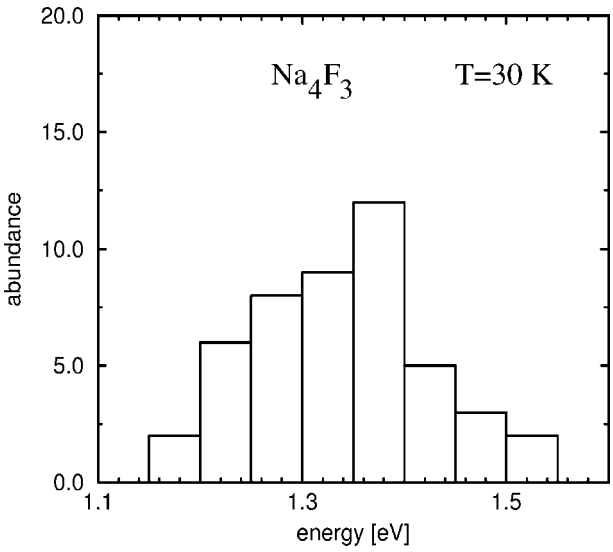

FIGURE 7. Franck–Condon profiles represented as a histogram of the energy gaps between the first excited electronic state and the ground state of a 30 K initial ensemble of Na_4F_3.

transition energy in the minimum of the first excited state; and (3) $E_{du} = 0.8$ eV corresponds to an intermediate value. The time between the first maxima of the signals calculated for $E_{du} = 1.2$ eV and $E_{du} = 0.6$ eV corresponds to the geometric relaxation time from the initially cuboidal structure (A) to the minimum of the first excited state ["cage" structure (B)] which amounts to less than 100 fs indicating a very fast configurational relaxation. Furthermore, both the $E_{du} = 1.2$ eV-signal and the $E_{du} = 0.8$ eV-signal exhibit strong oscillations with a period of 260 fs, thus these signals are sensitive to dynamical processes connected with the cage opening mode. In particular, the amplitudes of the maxima of the $E_{du} = 1.2$ eV-signal (cf. Fig. 9) are decreasing during the time evolution of the system, indicating that the reversion to the cuboidal structure is less likely to be accomplished from one oscillation period to the other. The reason for this is the restricted energy leaving IVR of the cage opening mode which was introduced above. From the decrease of the signal, we can roughly estimate the timescale for this type of IVR of about 1 ps. The "minimum-region" signal ($E_{du} = 0.6$ eV) is aperiodic after 1 ps, and the intensity increases significantly, indicating that the phase space occupation in the minimum of the first excited electronic state (open cage structure (B) in Fig. 9) raises during the propagation caused by the energy flow into this region. Note that this restricted energy arriving IVR differs from the one-mode selective energy, leaving IVR of the cage opening mode since the "minimum-region" signal cannot be attributed to one specific vibrational mode in contrast to the $E_{du} = 1.2$ eV signal. Consequently, the timescales of both IVR processes are different. However, as can be seen from Figure 9, the simulation time of 2 ps is too short in order to determine the timescale for restricted energy arriving IVR. Finally, the average amplitudes of the oscillations of the $E_{du} = 0.8$ eV signal remain almost constant. This indicates that a somewhat constant part of the phase space volume oscillates periodically above the minimum structure (B). However, the modulation of the oscillations in the $E_{du} = 0.8$ eV signal is due to either the anharmonicity of the cage opening mode or resonant IVR which arises from the coupling of the other modes to the still dominant cage opening mode. We wish to emphasize that, although the system has 15 degrees of freedom, no features of dissipative IVR could be found during the propagation time of 2 ps and for low initial temperature. This analysis of the restricted IVR processes may be important for the development of mode selective control mechanisms of these or similar systems with metallic-ionic and metallic-covalent bonds.

Simulation and Analysis of the NeExPo fs Pump-Probe Signals of Na_3F_2

First we present the optical response and structural properties of the ground and the first excited states of Na_3F_2, then characterize the conical intersection, and finally address dynamics involving passage through conical intersection.

The optical response properties obtained for both isomers of Na_3F_2 are shown in Figure 10 and compare well with those calculated, taking into account all valence electrons in our previous work [27, 28]. The lowest energy isomer I with the ionic Na_2F_2 subunit to which the Na atom is bound forming Na–Na and Na–F bonds gives rise to the low energy intense transition located at 1.33 eV. This is a common feature found for Na_nF_{n-1} clusters due to the localization of the one-excess electron either at the Na atom (e.g., in Na_2F and Na_3F_2) or at the F-deficient site (e.g., in Na_4F_3). In contrast, the transition to the first excited state of isomer II (C_{2v}) with the Na_3 subunit which is bridged by two F atoms has the energy of ~1.7 eV being close to the location of transitions arising from excitations in metallic

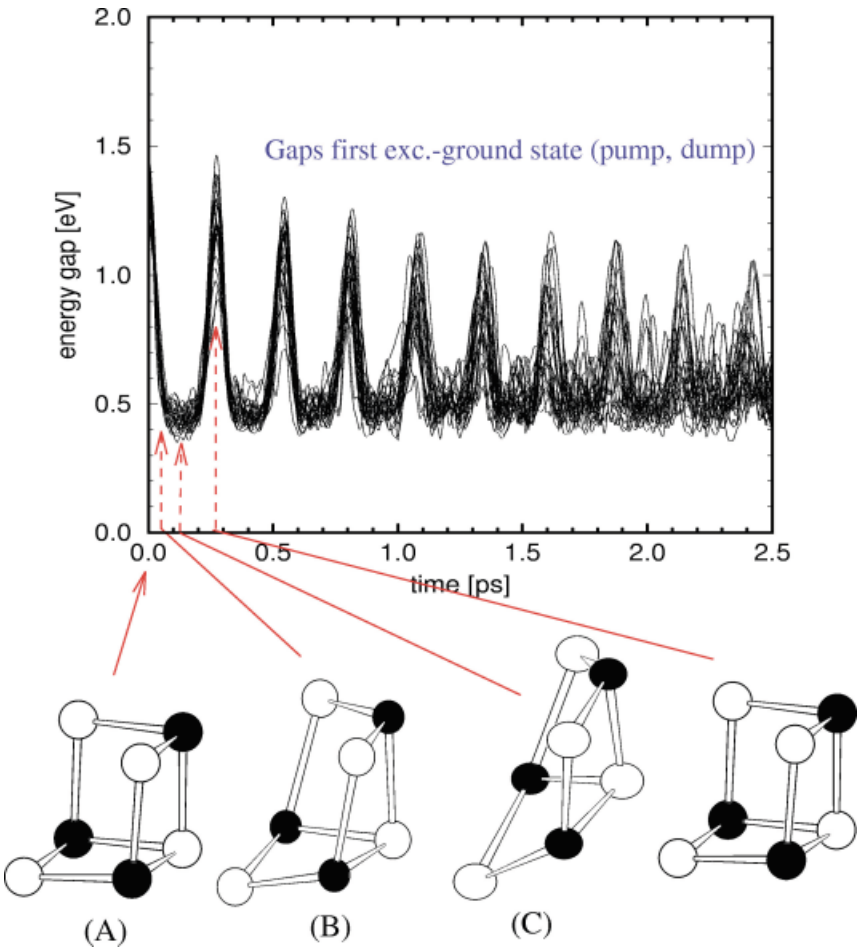

FIGURE 8. Bunches (30 trajectories) of energy gaps between the first excited and the ground state obtained from the dynamics on the first excited electronic state initiated by a pump excitation of a 30 K ensemble of Na_4F_3.

subunits. After the vertical transition at the geometry of the isomer I, the geometric relaxation in the first excited state takes place involving a breaking of the Na–Na bond leading to the first local minimum of the excited state [cf. Fig. 11, structure (A)] with a lowering of the energy by ∼0.17 eV. Afterward, the relaxation process proceeds to the absolute minimum with the linear geometry [cf. Fig. 11, structure (B)] corresponding to the conical intersection for which a further decrease of energy by ∼0.50 eV takes place. The linear geometry of the conical intersection is also reached after vertical transition to the first excited state at the geometry of the second isomer with C_{2v} structure. Thus, the investigation of the dynamics in the first excited state involves the breaking of metallic and ionic bonds starting from isomer I, and metallic bonds starting from isomer II, as well as the passage through the conical intersection.

As a consequence, one expects strong thermal motions within the ensemble leading to phase space spreading and IVR. All processes can be monitored by a second ionizing probe pulse with excitation energies between ∼2.9 eV and ∼4.8 eV, as shown by the *NeExPo* scheme given on Figure 12. The first value is close to the initial Franck–Condon transition region, and probes the relaxation dynamics on the first excited electronic state before the branching process due to the conical intersection occurs, while the latter value allows to monitor the processes involved in the ground state dynamics after the passage through the conical intersection.

We have used the algorithm introduced by Robb et al. [43] for the determination of the linear struc-

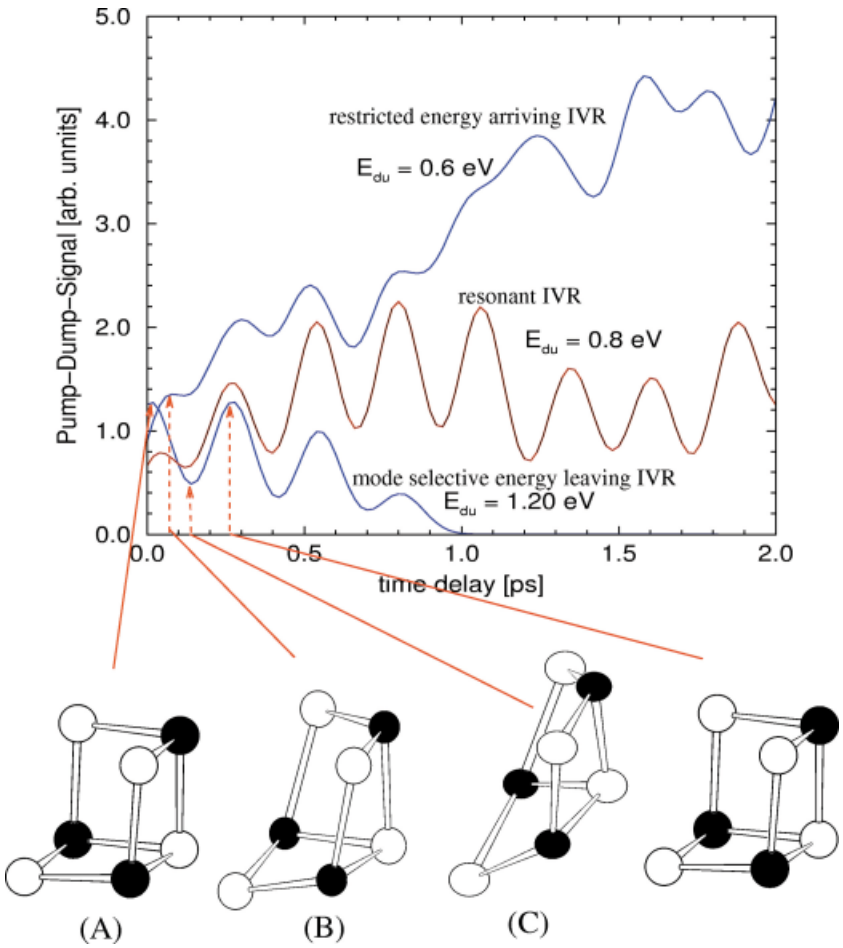

FIGURE 9. Simulated pump-dump signals of a 30 K initial ensemble of Na_4F_3 for three different excitation energies of the dump laser. Maxima and minima of the signals can be attributed to the given structures below.

ture (cf. Fig. 11) and the corresponding energy associated with the intersection point. Moreover, this algorithm also allows us to analyze the topology of the intersection in the space spanned by the internal degrees of freedom. The results obtained for Na_3F_2, which has $N = 10$ internal degrees of freedom, show that displacements in eight out of the ten directions almost do not change the energetic separation of the surfaces, while displacements in the orthogonal plane characterized by two directions X_1 and X_2 strongly remove the energy degeneracy. The X_1 is the gradient difference vector and X_2 involves the coupling vector between the states. In other words, the ground state reaction paths starting in the plane X_1X_2 connects the excited state reactants with the two ground state products. Thus, the intersection of the ground and the first excited state has the shape of a double cone with respect to X_1 and X_2, where the apex spans an eight-dimensional hyperline along which the energy is degenerate. The intersection seam is therefore (N-2) dimensional as it is characteristic for *conical intersections*.

The analysis of the wavefunctions of the ground and the first excited state in the close neighborhood of the conical intersection yields positive and negative linear combinations of two "valence bond like" structures $Na^+–F^––Na^+–F^––\dot{N}a \pm \dot{N}a–F^––Na^+–F^––Na^+$, with one of them contributing dominantly to the ground and the other one to the first excited state, thus giving rise to two states with different symmetry. The location of the excess electron is indicated by the dot above the sodium atom. Of course, at the point of conical intersection, the arbitrary

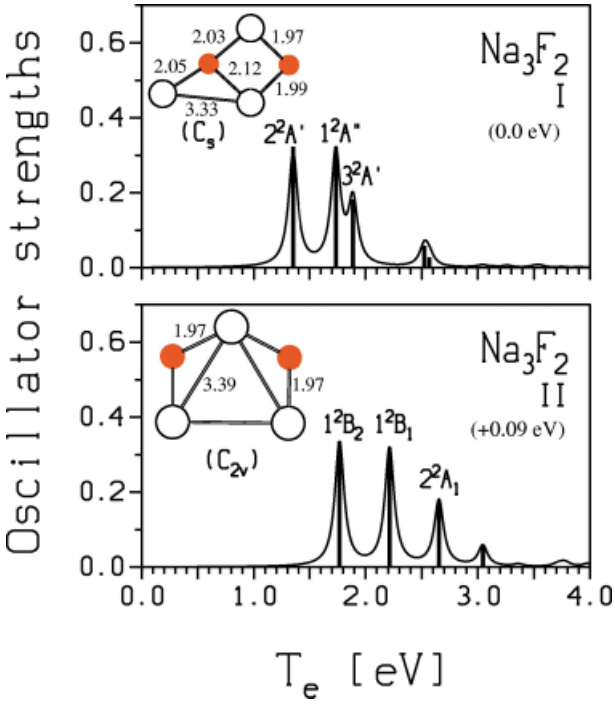

FIGURE 10. Optically allowed transitions T_e in eV and oscillator strength f_e obtained from the one-electron "frozen ionic bonds" approximation for the stable ground state isomer I and the second isomer II of Na_3F_2 which has ~0.09 eV higher energy. Bond lengths of the structures are indicated in Å.

linear combination of the above "valence bonds" structures is possible due to the degeneracy. The two "VB" structures differ in the translocation of the single excess electron or the charge from one end to the other of the linear system. In other words, the length of the linear chain is sufficiently long to allow for energy gap closing in analogy to the dissociation limit of the H_2^+ molecule for which the degeneracy of the ground and excited state occurs due to equal energies of $\dot{H}$ $-H^+$ and H^+- $\dot{H}$ structures. This means that in the case that the linear molecule is not sufficiently long to minimize the repulsion, avoided crossing will take place as in the case of Na_2F, which turns into the conical intersection for Na_3F_2. In other words, the presence of the conical intersection in the latter case through which the isomerization process can take place is the consequence of the electronic structure, and therefore has a general nature which can be found for other systems by designing the analogic electronic situation. Therefore, this finding is of general importance.

In fact, the analogy can be drawn to conical intersections found in photochemistry involving biradicaloid species, which arise by partial breaking of double hetero bonds due to geometric relaxation in the singlet excited states. The condition for the occurrence of conical intersections in so-called "critical biradicals" has been formulated in the framework of a two-orbital two-electron model and can be fulfilled in the case that the electronegativity difference between the two centers is sufficient to minimize the repulsion between the ground and the excited states [44–47]. This occurs in the protonated Shiff bases by twisting the chromophore $H_2C–N^+H_2$ bond leading to cis-trans isomerization. In this case, the ground and excited states at the conical intersection are characterized by "VB" structures $H_2\dot{C}–\dot{N}^+H_2$ and $H_2C^+–\ddot{N}H_2$ which differ in translocation of charge from one to the other center of the chromophore [38–41]. In fact, experimentally it has been confirmed that the conical intersection is responsible for the cis-trans isomerization of the retinal chromophore in the vision process [48–50].

However, the investigation of the nonadiabatic dynamics through the conical intersection of Na_3F_2 has advantages. The system has 10 degrees of freedom and permits the calculation of an ensemble of trajectories based on the accurate ab initio description of the excited and ground electronic states and corresponding MD, thus providing the conceptual framework for fs-observables such as fs pump-probe signals which will be addressed below.

In order to obtain initial conditions, we have assumed a canonical thermal ensemble of 50 K which is determined by the Wigner distribution function of the electronic ground state including all normal modes ω_i, $i = 1,\ldots,10$, of the C_s structure corresponding to the total minimum of energy. The set of 100 initial conditions were obtained by sampling the Wigner distribution function with respect to the coordinates $\mathbf{q}_0$ and momenta $\mathbf{p}_0$ which were used for the classical trajectory simulations on the first excited state of Na_3F_2. The finite temperature of 50 K causes thermal deviations from the energy minimum C_s structure which have been characterized by the histogram of abundances of the energy gaps between the first excited electronic state and the ground state shown in Figure 13. The maximum

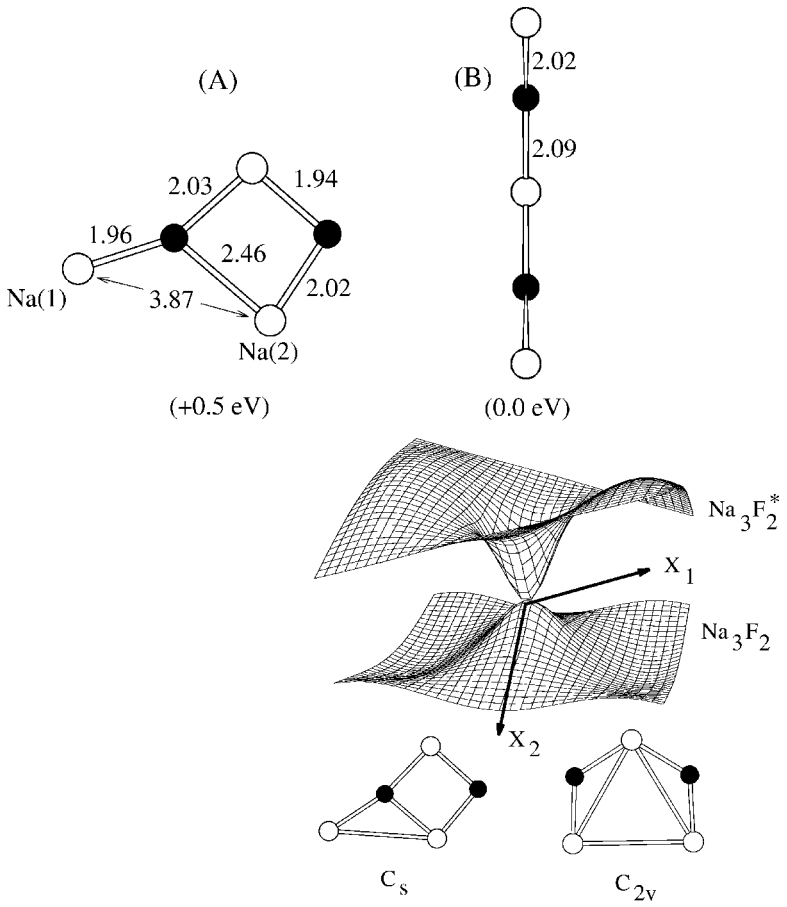

FIGURE 11. Structures corresponding to the minimum on the first excited state of Na_3F_2 (A) involving a broken bond between Na(1) and Na(2) which lies 0.5 eV above the linear minimum energy structure of the conical intersection (B). Bond lengths are indicated in Å. The lower part shows a sketch of the conical intersection region between the first excited state ($Na_3F_2^*$) and the ground state characterized by the two vectors X_1 and X_2, where the apex of the double cone spans an eight-dimensional seam. The minima on the ground state surface correspond to the C_s and the C_{2v} structure, respectively.

at ~1.35 eV corresponds to the energy gap value at the C_s structure of Na_3F_2.

Next we wish to outline important parts of the analysis of the nuclear dynamics. The simulation of the classical trajectory ensemble consisting of the 100 sampled phase space points has been started on the first excited electronic state. The geometric relaxation toward the linear structure corresponding to the conical intersection, its passage, as well as the subsequent relaxation dynamics on the electronic ground state can be visualized by considering the phase space density of the cluster ensemble shown in Figure 14 for different propagation times. At the beginning, $t = 0$ fs, the phase space density is localized corresponding to the C_s structure [cf. Fig. 14(a)]. During the subsequent ~90 fs, the distance between the Na(1) and Na(2) atoms elongates by about 25%, indicating the bond breaking between both sodium atoms [cf. Fig. 14(b)]. Consecutive ionic bond breaking between the Na(2) and the F(2) atoms can be observed after 220 fs [cf. Fig. 14(c)], together with a small delocalization of the phase space density. After ~400 fs, the region of the conical intersection corresponding to the linear structure is reached [cf. Fig. 14(d)] which triggers the branching of the phase space density from the excited electronic state to the ground state. At this stage, the system gained an additional kinetic energy of ~0.67 eV. Due to this large vibrational excess energy, strong anharmonicities be-

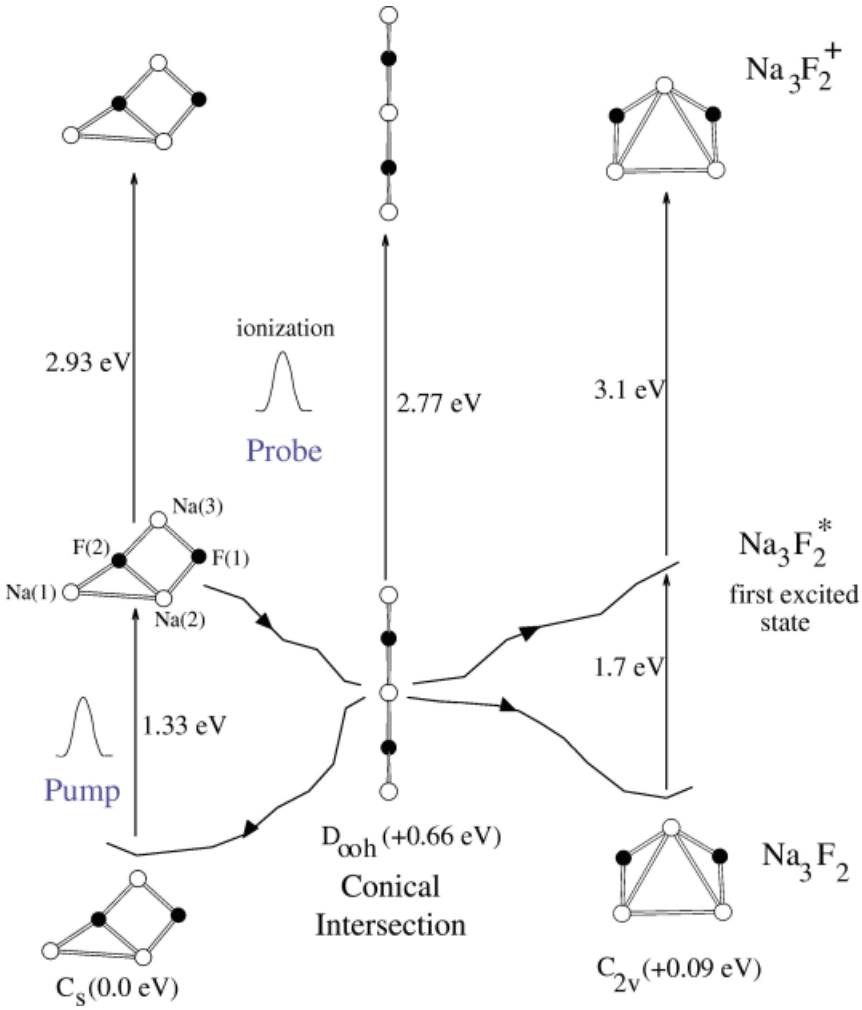

FIGURE 12. Scheme of the multistate fs dynamics of Na_3F_2 in the framework of the *NeExPo* pump-probe spectroscopy. The dynamics on the first excited electronic state from the initially C_s geometry after vertical transition toward the linear minimum energy structure of the conical intersection region, as well as the branching to the ground state leading to both the C_s and the C_{2v} structure, are indicated by thick arrows. Transition energies between the ground and excited state, as well as between the cationic and the excited state, are given by thin arrows. All corresponding geometries are drawn.

tween the vibrational modes must be present which are responsible for the phase space spreading. The subsequent relaxation dynamics on the electronic ground state are characterized by an even larger phase space spreading, particularly after 1000 fs since the vibrational excess energy rose to ~1.3 eV which would correspond to an equilibrium temperature of ~3400 K (cf. Fig. 14(e)–(l)]. However, although there is increasing phase space spreading, one can clearly gain structural information of the cluster ensemble up to a propagation time of ~1000 fs by considering the center of mass positions of the atomic phase space distributions in Figure 14(e)–(i). In particular, the "center of mass geometry" at 800 fs is close to the C_{2v} structure, but due to the phase space spreading there are also considerable deviations, and even geometries close to the C_s structure are involved in the phase space distribution of the cluster ensemble. As will be shown below, one can obtain detailed information about the ratio between these structures as well as energetic distributions in the cluster ensemble from pump-probe signals. For times beyond 1 ps, no structures can be identified in the phase space distribution [cf. Fig. 14(j)–(l)], thus the ensemble is geometrically completely delocalized at least up to

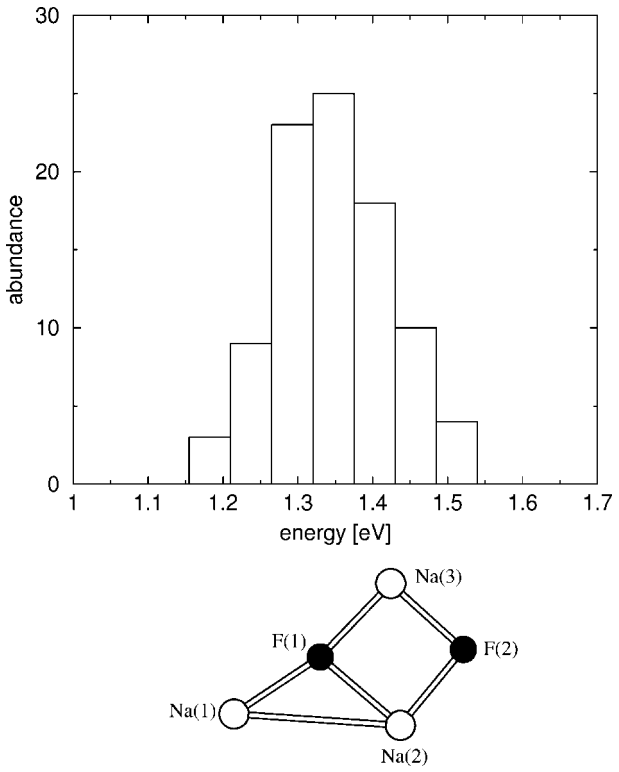

FIGURE 13. Histograms of the energy gaps (transition energies) between the first excited electronic state and the ground state of Na_3F_2 for a 50 K initial temperature ensemble obtained from 100 sampled phase space points of the canonical Wigner distribution. The maximum of the histogram corresponds to the transition energy for the stable ground state isomer I (C_s) shown below.

the propagation time of 2.5 ps, which is understandable due to the large vibrational excess energy of ~1.3 eV.

In addition, we have investigated the time-dependent velocity autocorrelation function which provides additional information about the dynamics. As can be clearly shown from Figure 15, there are regular oscillatory features before the conical intersection is reached at ~400 fs. The period of ~95 fs can be attributed to a normal mode of the C_s structure at 349 cm^{-1} (cf. Table II) corresponding to a stretching motion between Na(2) and F(1) (for the meaning of the labels, cf. Fig. 13). Thus, one can conclude that the large amplitude motion of the Na(2)-atom toward the linear structure of the cluster leading to an opening of the Na_2F_2 rhombic subunit involves the bond breaking of the metallic Na(1)–Na(2) bond and the ionic Na(2)–F(2) bond as well as the elongation of the remaining Na(2)–F(1) ionic bond. After the passage through the conical intersection, the oscillations disappear and the amplitude of the velocity autocorrelation function vanishes beyond 1 ps. This behavior corresponds to the fact that the ensemble is structurally and energetically delocalized after 1 ps, as was discussed in the context of the phase space distribution (cf. Fig. 14).

In summary, we wish to emphasize that the dynamics through the conical intersection represent an elementary physical event for the cluster ensemble in the sense that it initiates the transition from structurally and energetically localized behavior involving consecutive metallic and ionic bond breaking processes to delocalized behavior, which destroys the correlations in the system since the autocorrelation function vanishes. Thus, the molecular dynamics can be divided into a reversible and an irreversible part separated by the passage through the conical intersection.

Finally, we have simulated *NeExPo* pump-probe signals according to Eq. (6) using energy gaps obtained from the classical trajectory simulations based on the fewest switching hopping algorithm for the ensemble of 50 K initial temperature. In order to obtain comprehensive information on the dynamical processes of Na_3F_2, zero pump pulse duration ($\sigma_{pu} = 0$) involving a complete excitation of the ground state ensemble prepared at the initial temperature was assumed. However, a probe pulse duration of 50 fs was chosen, which allows us to resolve the ultrafast structural relaxation processes involving the bond breaking. The simulations of the signals have been performed for four different excitation energies (wavelengths) of the probe pulse (cf. Fig. 16).

- $E_{pr} = 2.8$ eV and $E_{pr} = 3.0$ eV correspond to transition energy values between the first excited and the cationic state at the time of the Na–Na metallic and the Na–F ionic bond breaking, respectively. Thus the signals for the above transition energies provide the information on the structural relaxation involving the bond breaking processes in the first excited state of Na_3F_2 before the conical intersection is reached. In fact, they exhibit maxima at ~90 fs and ~220 fs [cf. Fig. 16(a)] in agreement with the timescales for the metallic and ionic bond

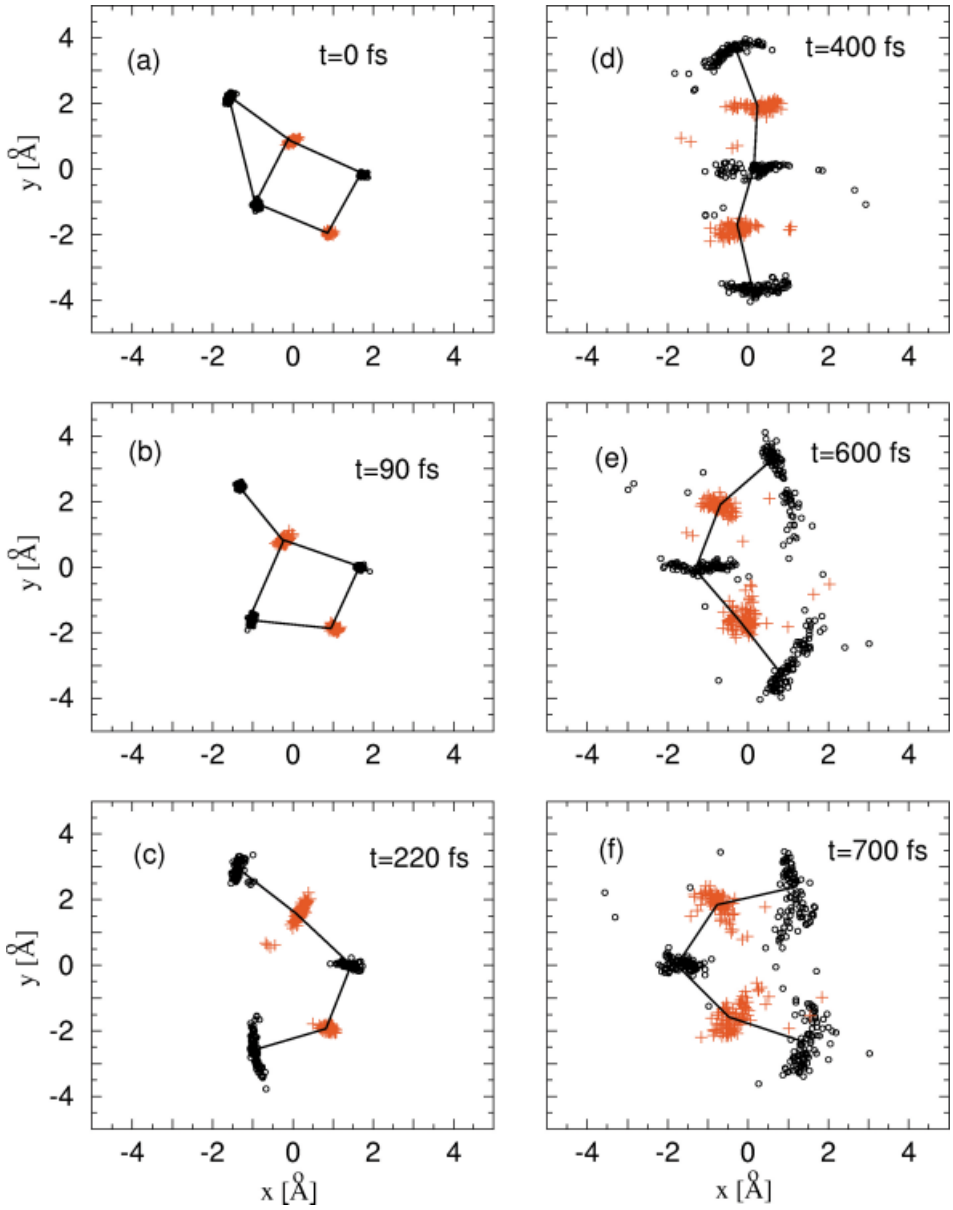

FIGURE 14. Snapshots of the phase space distribution (PSD) consisting of 100 phase space points obtained from classical trajectory simulations based on the fewest-switching surface hopping algorithm of a 50 K initial canonical ensemble. Na-atoms are indicated by black circles and F-atoms by gray crosses. (a)–(d) Dynamics on the first excited state starting at the C_s structure (a) proceeds over the structure with broken Na–Na bond (b), and subsequently broken ionic Na–F bond (c) toward the conical intersection region (d). (e)–(l) Dynamics on the ground state after branching of the PSD from the first excited state lead to strong spatial delocalization. The C_{2v} isomer can be identified between 800 and 900 fs [(g), (h)] in the "center of mass" distribution.

breaking obtained from the analysis of the phase space distribution and energy gap values. Both signal intensities decrease rapidly after 0.4–0.5 ps, indicating the branching of the phase space density from the first excited electronic state to the ground state due to the conical intersection.

- E_{pr} = 4.3 eV and E_{pr} = 4.8 eV [cf. Fig. 16(b)] correspond to transition energies between the ground state and the cationic state at the C_s

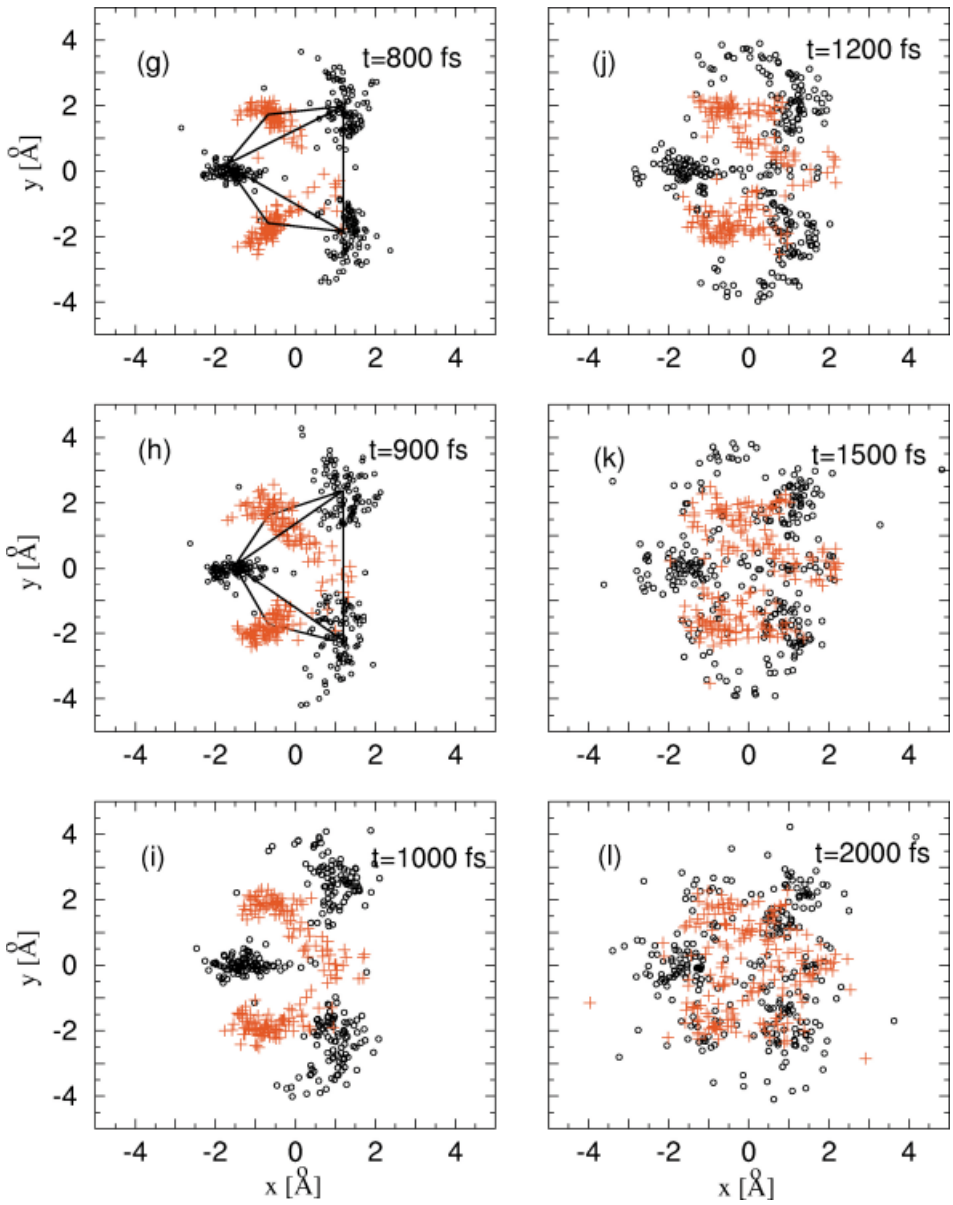

FIGURE 14. (Continued)

geometry and the C_{2v} geometry (cf. scheme on Fig. 12), respectively. In such a way, the signals monitor the ratio of both isomers in the phase space distribution after the passage through the conical intersection up to a time delay between pump and probe of ~1 ps. This time represents the limit up to which structural information can be resolved in the phase space distribution (cf. Fig. 14). For larger time delays, the signals provide only information about the energetic redistribution, i.e., IVR. In fact, the intensities of both signals start to increase after ~0.4 ps since the ground state becomes populated providing the timescale for the passage of the conical intersection [cf. Fig. 16(b)]. Furthermore, the signal at $E_{pr} = 4.8$ eV exhibits a maximum at 0.8–0.9 ps indicating the larger ratio of the C_{2v} structure in correspondence with the results obtained from the phase space distribution

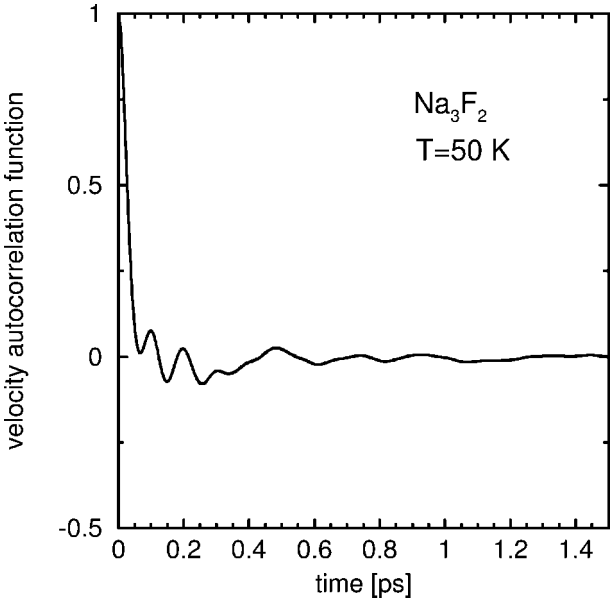

FIGURE 15. Time-dependent velocity autocorrelation function obtained for the dynamics of the 50 K initial temperature Na_3F_2 ensemble.

[cf. Fig. 14(g)]. This signal drops rapidly after 0.9 ps, and the signal at $E_{pr} = 4.3$ eV increases indicating that the C_s structure is more populated at 0.9–1.0 ps [cf. Fig. 16(b)].

The latter one also exhibits oscillatory features beyond 1 ps, i.e., corresponding to the IVR regime, which leads to the conclusion that a somewhat periodic energy flow is present in the cluster ensemble. Of course, due to the high vibrational excess energy, these oscillations cannot be attributed to particular normal modes. These results show that different physical processes are involved in the dynamics of Na_3F_2 cluster initiated by the Frank–Condon pump pulse transition to the first excited electronic state, such as geometric relaxation, consecutive bond breaking of metallic and ionic bonds, passing through the conical intersection, and IVR processes. Moreover, the timescales of these processes can be identified in *NeExPo* signals, and each of them can be selectively monitored by tuning of the probe excitation energy.

Conclusion

We have shown that the combination of the ab initio multistate MD "on the fly" involving ground and excited electronic states, including nonadiabatic coupling and the Wigner distribution approach for simulating the time resolved pump-probe and pump-dump fs signals, is suitable for the description of different types of relaxation processes and for the determination of their timescales. This approach is able to reproduce the available experimental results, to predict under which experimental conditions different processes such as configurational relaxation and IVR can take place and to study the nature of these processes. The investigation on Na_nF_{n-1} clusters allows to identify in pump-dump or pump-probe signals geometrical changes, breaking of bonds, isomerization, conical intersection, IVR and their nature (e.g., one-mode selective energy leaving IVR, resonant and restricted energy arriving IVR) in the context of varying the cluster size and their structural and electronic properties. Moreover it serves as stimulation for experimental work and for further development of theoretical methods and concepts.

Appendix A: Excited States Energies, Their Analytic Derivatives, and Adiabatic Molecular Dynamics

We present the "frozen ionic bonds" approximation, pointing out its advantages for the calculation of transition energies and mainly for carrying out the MD "on the fly" involving low-lying excited states. The Na_nF_{n-1} clusters are characterized by a large energy gap between the HOMO-1 and LUMO orbitals (∼14 eV), while the HOMO orbital occupied by the single excess electron lies roughly ∼10 eV above HOMO-1 [27]. This situation is suitable to introduce the "frozen ionic bonds" approximation for $n-1$ electrons involved in ionic bonding [28]. This allows us to describe the ground state of the system on the restricted open shell Hartree–Fock (ROHF) level, yielding canonical MOs φ_i. The excited states are obtained as eigenstates of an effective one-excess electron Hamiltonian containing Coulomb and exchange operators with the core defined as

$$\hat{h}' = \hat{h} + \sum_{c<o} \left[2\hat{J}_c(1) - \hat{K}_c(1)\right] \qquad \text{(A–1)}$$

where the sum extends over all doubly occupied orbitals c (o labels the open shell single occupied HOMO), i.e., over the atomic cores as well as over the bonding orbitals corresponding to the ionic bonds. The operators $\hat{h}$, $\hat{J}_c$, and $\hat{K}_c$ are the one-electron part of the total Hamiltonian, the Coulomb,

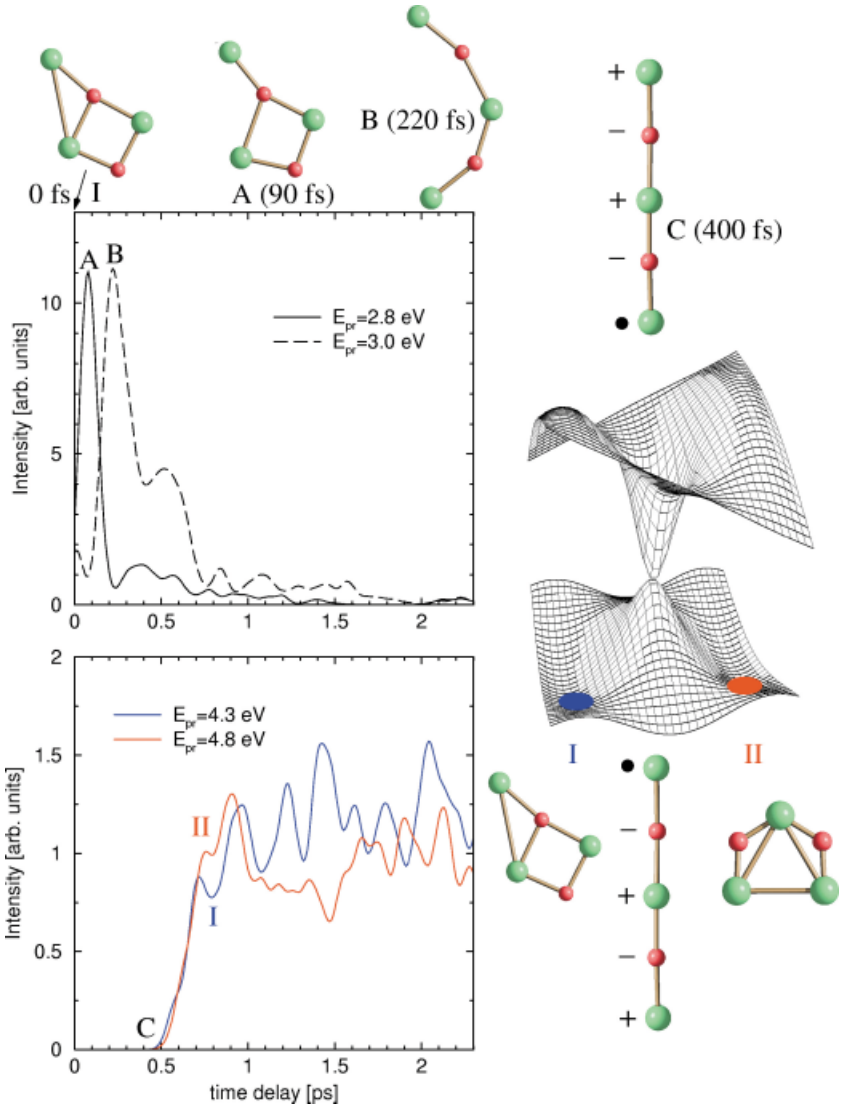

FIGURE 16. Simulated *NeExPo* pump-probe signals for the 50 K initial temperature Na_3F_2 ensemble at different excitation energies of the probe laser allowing us to monitor geometric relaxation on the first excited state involving bond breaking processes and passage through the conical intersection, as well as geometric relaxation and IVR processes on the ground state after the passage.

and the exchange operators (with respect to the ionic bonds), respectively.

The corresponding matrix elements in the MO basis φ_i read

$$h'_{ji} = h_{ji} + \sum_{c<o} [2(ji|cc) - (jc|ci)] \qquad (j,i = o,\ldots,M) \tag{A–2}$$

where h_{ji} are one-electron integrals, and $(ji|cc)$ and $(jc|ci)$ are two-electron integrals in the MO basis (containing M functions). The indices j,i run only through the HOMO and virtual orbitals, since the lower ones are already occupied and correspond to the "frozen" ionic bonds. Eq. (A–2) is identical to the expression for the closed shell Fock matrix (constructed from the MOs of the neutral open shell one-excess electron system φ_i)

$$F^{MO}_{ki} = h_{ki} + \sum_{j<o} [2(ki|jj) - (kj|ji)] \qquad (i,k = 1,\ldots,M) \tag{A–3}$$

except for the range of indices k, i. Therefore, the matrix of the one-excess electron Hamiltonian $\boldsymbol{h}'$ is just a submatrix of the Fock matrix (A–3) and can be obtained straightforwardly by modifying the standard self-consistent field (SCF) program in such way that after the convergence of neutral restricted open shell Hartree–Fock (ROHF) SCF procedure is achieved, one additional closed-shell SCF iteration can be performed yielding the closed shell Fock matrix. In analogy, the code for the Fock matrix derivative can be modified to compute derivatives of the $\boldsymbol{h}'$ matrix elements.

The wavefunctions ψ_i of the individual states of the one-excess electron are then obtained as eigenfunctions of $\hat{h}'$ and can be expressed as

$$\psi_i = \sum_{j=o}^{M} D_{ji}\varphi_j \qquad (i = o, \ldots, M) \tag{A–4}$$

where $\boldsymbol{D}$ is an unitary matrix which diagonalizes $\boldsymbol{h}'$

$$\boldsymbol{h}'\boldsymbol{D} = \boldsymbol{D}\boldsymbol{E}, \qquad \boldsymbol{E} \equiv \mathrm{diag}(\epsilon_i). \tag{A–5}$$

The eigenvalues ϵ_i are the energies of the one-excess electron, and their differences correspond to transition energies. Therefore, the total energy of an excited state has the following form:

$$E_i = E_{SCF} + \epsilon_i - \epsilon_o, \tag{A–6}$$

where ϵ_o is the ground state energy of the one-excess electron. Note that despite the fact that the energy difference $\epsilon_i - \epsilon_o$ might resemble a simple Koopmans theorem, the energy levels of the excess electron ϵ_i are (with the exception of ϵ_o) not equal to the SCF MO energy levels. They correspond to solution of excited states of the one-excess electron, which feels the constant field of the remaining electrons, being "frozen" in the ground state.

The eigenvectors D_{ji} are used to obtain the transition density matrix $\gamma_{h,l}(jk)$ between hth and lth states

$$\gamma_{h,l}(j,k) = D^*_{jh} D_{k\ell}, \tag{A–7}$$

from which transition moments and, subsequently, the oscillator strengths are computed. The total computational cost for the calculation of the absorption spectrum involving the transition energies and oscillator strengths amounts to the ROHF calculation, the single closed-shell iteration, and a few matrix multiplications needed for the calculation of transition moments. A comparison between the, spectra of Na_2F and Na_4F_3 obtained from the MRCI [27, 28] method correlating all electrons and those obtained from the "frozen ionic bonds" approximation is given in Table I, which confirms the accuracy of the latter.

For the calculation of the gradient of the total energy given by Eq. (A–6), in addition to the gradient of the ROHF SCF energy, the derivatives of the excess electron energies $\nabla_{\boldsymbol{R}}\epsilon_i$ are needed. Using the definition of the orbital energies ϵ_i

$$\epsilon_i = \langle \psi_i h' \psi_i \rangle \tag{A–8}$$

$$= \sum_{j,k} (D^\dagger)_{ij} h'_{jk} D_{ki} \tag{A–9}$$

one obtains

$$\nabla_{\boldsymbol{R}}\epsilon_i = \sum_{jk} \big[(\nabla_{\boldsymbol{R}} D^\dagger)_{ij} h'_{jk} D_{ki} + (D^\dagger)_{ij} h'_{jk} \nabla_{\boldsymbol{R}} D_{ki} + (D^\dagger)_{ij} (\nabla_{\boldsymbol{R}} h'_{jk}) D_{ki} \big] \tag{A–10}$$

$$= \sum_{j} \epsilon_i \big[(\nabla_{\boldsymbol{R}} D^\dagger)_{ij} D_{ji} + (D^\dagger)_{ij} \nabla_{\boldsymbol{R}} D_{ji} + \big] + \sum_{jk} (D^\dagger)_{ij} (\nabla_{\boldsymbol{R}} h'_{jk}) D_{ki}. \tag{A–11}$$

Since the term in brackets corresponds to a derivative of the normalization condition

$$\sum_{jk} (D^\dagger)_{ij} D_{jk} = \delta_{ik}, \tag{A–12}$$

it remains only second term

$$\nabla_{\boldsymbol{R}}\epsilon_i = \sum_{jk} (D^\dagger)_{ij} (\nabla_{\boldsymbol{R}} h'_{jk}) D_{ki}, \tag{A–13}$$

which requires the calculation of derivatives of the effective one-excess electron Hamiltonian $\nabla_{\boldsymbol{R}} h'_{jk}$. They are identical to the derivatives of the closed shell Fock-matrix $\boldsymbol{F}$ obtained from the cation with the converged orbitals of the neutral system. The gradient

$$\nabla_{\boldsymbol{R}} h'_{ij} = \nabla_{\boldsymbol{R}} h_{ij} + \sum_{c} \big[2\nabla_{\boldsymbol{R}} (ij|cc) - \nabla_{\boldsymbol{R}} (ic|cj) \big] \tag{A–14}$$

is therefore reduced to known expressions (cf. [32]).

$$\nabla_{\boldsymbol{R}} h'_{ij} = h'^{\boldsymbol{R}}_{ij} + \sum_{k} \big(U^{\boldsymbol{R}}_{ki} h'_{kj} + U^{\boldsymbol{R}}_{kj} h'_{ik} \big) + \sum_{k} \sum_{l} U^{\boldsymbol{R}}_{kl} A_{ij,kl} \tag{A–15}$$

$$h'^{\boldsymbol{R}}_{ij} = h^{\boldsymbol{R}}_{ij} + \sum_{k} \big\{ 2(ij|kk)^{\boldsymbol{R}} - (ik|jk)^{\boldsymbol{R}} \big\} \tag{A–16}$$

$$A_{ij,kl} = 4(ij|kl) - (ik|jl) - (il|jk). \tag{A–17}$$

In the above equations, the summations over k, l indices run from 1 to M, while i, j indices are confined to $o, \ldots, M$. The quantities $U^{\boldsymbol{R}}_{kl}$ in Eq. (A–15) describe

the influence of geometry changes on the SCF eigenvectors $C_{\alpha i}$ which are defined as

$$\nabla_R C_{\alpha i} = \sum_{j=1}^{M} C_{\alpha j} U_{ji}^R \tag{A–18}$$

and are obtained as solutions of the extended general restricted open-shell coupled perturbed Hartree–Fock equations (CPHF) which are part of program packages for computation of analytic second derivatives of the ROHF energy [32]. Notice that the "extended" CPHF equations are needed in order to obtain the U_{ki}^R quantities where the k, i indices may correspond both to occupied or to virtual orbitals, which are not necessary for analytic second derivatives of the ROHF energy. The appropriate computational procedure is described in Refs. [35, 36]. The quantities h_{ij}^R, $(ij|kk)^R$, $(ik|jk)^R$ in Eq. (A–16) represent derivatives of one- and two-electron integrals in the AO basis, transformed into the MO basis (not including derivatives of the SCF eigenvectors)

$$h_{ij}^R = \sum_{\mu\nu}^{AO} C_{\mu i} C_{\nu j} \nabla_R h_{\mu\nu} \tag{A–19}$$

$$(ij|kl)^R = \sum_{\mu\nu\rho\sigma}^{AO} C_{\mu i} C_{\nu j} C_{\rho k} C_{\sigma l} \nabla_R (\mu\nu|\rho\sigma). \tag{A–20}$$

To summarize, the derivative of the effective one-excess electron Hamiltonian can be built just like the derivative of the Fock matrix in CPHF for a closed shell system (of the cation), but using the SCF eigenvectors $C_{\alpha j}$ and the U_{ji}^R coefficients obtained from an ROHF and extended CPHF calculation of the open shell neutral system.

Once the analytic gradient of the one-excess electron energy is known, the velocity Verlet time propagation algorithm can be employed in order to solve equations of motion

$$M\ddot{\boldsymbol{R}} = -\nabla_R E(\boldsymbol{R}(t)) \tag{A–21}$$

and to compute the classical trajectories of the nuclei in the adiabatic electronic excited states.

The calculation of excited state energies and of gradients based on the "frozen ionic bonds" approximation is, from a computational point of view, considerably less demanding than in the framework of other approaches such as RPA, CASSCF, or CI by achieving the same accuracy. Therefore, our approach allows us to carry out adiabatic molecular dynamics in the excited state, calculating the forces "on the fly" with low computational demand which is mandatory for constructing of an ensemble of trajectories. Moreover, the fast computation of the nonadiabatic couplings "on the fly" also allows us to carry out nonadiabatic MD, as will be shown in Appendix B. Of course, the application is limited to systems for which the "frozen ionic bonds" approximation offers an adequate description.

Appendix B: Nonadiabatic Couplings in the Framework of "Frozen Ionic Bonds" Approximation

The consideration of nonadiabatic effects in the molecular dynamics requires the calculation of the first-order nonadiabatic couplings $(\nabla_R)_{ij} \equiv \langle\psi_i|\nabla_R|\psi_j\rangle$.

The nonadiabatic couplings employing the expansion of the ψ_j functions into the MO basis φ_i (cf. Appendix A) contain two terms:

$$\langle\psi_j|\nabla_R|\psi_i\rangle = \sum_k D_{kj}^* \nabla_R D_{ki} + \sum_{kl} D_{lj}^* D_{ki} \langle\varphi_l|\nabla_R|\varphi_k\rangle \tag{B–1}$$

and we wish to outline the derivation of each of them.

The first right-hand side term involves the derivatives of the eigenvectors of the effective one-excess electron Hamiltonian matrix $\nabla_R D_{ki}$, which can be obtained from the derivative of the effective one-excess electron Hamiltonian $\nabla_R h'_{ij}$ (cf. Appendix A). For this purpose, we introduce the vector $\boldsymbol{E}$ for the diagonal matrix elements of eigenvalues ϵ_i of the Hamiltonian $\boldsymbol{h}'$, and $\boldsymbol{D}$ is the unitary matrix of the corresponding eigenvectors:

$$\boldsymbol{h}'\boldsymbol{D} = \boldsymbol{D}\boldsymbol{E} \tag{B–2}$$

$$\boldsymbol{D}^\dagger\boldsymbol{D} = \boldsymbol{1}. \tag{B–3}$$

The derivative of the eigenvalues can be obtained by multiplying Eq. (B–2) by $\boldsymbol{D}^\dagger$ from the left and performing the derivative (taking into account that the derivative of the normalization condition (B–3) is zero):

$$(\nabla_R \boldsymbol{E})_{ii} = (\boldsymbol{D}^\dagger \nabla_R \boldsymbol{h}' \boldsymbol{D})_{ii}. \tag{B–4}$$

Notice that Eq. (B–4) holds only for the diagonal elements of the matrix $\boldsymbol{E}$, while an analogous equation for the whole matrix $\nabla_R \boldsymbol{E}$ is not valid.

In order to obtain the derivative of eigenvectors $\nabla_R \boldsymbol{D}$, we search for the solution in the following form:

$$\nabla_R \boldsymbol{D} = \boldsymbol{D}\boldsymbol{X}. \tag{B–5}$$

Since $\boldsymbol{D}$ is unitary, $\boldsymbol{X}$ is uniquely defined and the derivative of the normalization condition (B–3) implies the antihermiticity of $\boldsymbol{X}$:

$$\boldsymbol{X}^\dagger + \boldsymbol{X} = \boldsymbol{0}. \tag{B–6}$$

Performing the derivative of Eq. (B–2)

$$(\nabla_R \boldsymbol{h}')\boldsymbol{D} + \boldsymbol{h}'(\nabla_R \boldsymbol{D}) = (\nabla_R \boldsymbol{D})E + \boldsymbol{D}\nabla_R \boldsymbol{E}, \tag{B–7}$$

and multiplying this equation by $\boldsymbol{D}^\dagger$ from the left using Eqs. (B–2) and (B–5), one obtains

$$\boldsymbol{XE} - \boldsymbol{EX} = \boldsymbol{D}^\dagger(\nabla_R \boldsymbol{h}')\boldsymbol{D} - \nabla_R \boldsymbol{E} \equiv \boldsymbol{Y}. \tag{B–8}$$

The right-hand side matrix is labeled by $\boldsymbol{Y}$; it can be easily verified that it is Hermitian, and due to Eq. (B–4) it has zeros on its diagonal. Since the matrix $\boldsymbol{E}$ is diagonal, Eq. (B–8) can be explicitly solved for the matrix elements of $\boldsymbol{X}$

$$X_{ij} = \frac{Y_{ij}}{E_{jj} - E_{ii}} (i \neq j); \qquad X_{ii} = 0. \tag{B–9}$$

Notice that this equation is in agreement with the requirement of the antihermiticity of $\boldsymbol{X}$, Eq. (B–6). Furthermore, if the eigenvalues of the $\boldsymbol{h}'$ matrix are degenerate, the denominator in Eq. (B–9) becomes zero, which is in agreement with the fact that eigenvectors corresponding to the same eigenvalue are not uniquely defined. The explicit expression for the matrix elements of $\boldsymbol{X}$, Eq. (B–9), together with Eq. (B–5), yield the needed derivative of eigenvectors $\nabla_R \boldsymbol{D}$.

For the second right-hand side term of Eq. (B–1), we use the expansion from the MO basis into the AO one

$$\varphi_i = \sum_\alpha C_{\alpha i} \chi_\alpha \tag{B–10}$$

and obtain

$$\langle \varphi_j | \nabla_R | \varphi_i \rangle = \sum_{\alpha\beta} C^*_{\beta j} S_{\beta\alpha} \nabla_R C_{\alpha i} + \sum_{\alpha\beta} C^*_{\beta j} C_{\alpha i} \langle \chi_\beta | \nabla_R | \chi_\alpha \rangle \tag{B–11}$$

where $S_{\beta\alpha}$ is the overlap matrix, and the derivatives of the SCF eigenvectors $\nabla_R C_{\alpha i}$ can be obtained from the extended coupled perturbed Hartree–Fock coefficients $\boldsymbol{U}^R$ which have already been outlined for the adiabatic MD in Appendix A using Refs. [32–36]. The first right-hand side term in Eq. (B–11) thus simplifies in the matrix notation to

$$\boldsymbol{C}^\dagger \boldsymbol{S} \nabla_R \boldsymbol{C} = \boldsymbol{C}^\dagger \boldsymbol{S} \boldsymbol{C} \boldsymbol{U}^R = \boldsymbol{U}^R, \tag{B–12}$$

where the orthonormality of the SCF eigenvectors $\boldsymbol{C}^\dagger \boldsymbol{S} \boldsymbol{C} = \boldsymbol{1}$ has been used.

The evaluation of the second right-hand side term in Eq. (B–11) requires the integrals in the contracted Cartesian Gaussian AO basis:

$$\chi_\alpha = \sum_\gamma K_{\gamma\alpha} \phi_\gamma. \tag{B–13}$$

Since the contraction coefficients $K_{\gamma\alpha}$ are constant, the transformation to primitive basis ϕ_γ is simple:

$$\langle \chi_\beta | \nabla_R | \chi_\alpha \rangle = \sum_{\gamma\delta} K_{\gamma\alpha} K_{\delta\beta} \langle \phi_\delta | \nabla_R | \phi_\gamma \rangle. \tag{B–14}$$

The integrals in the primitive AO basis $\langle \phi_\delta | \nabla_R | \phi_\gamma \rangle$ vanish, unless the derivative is taken with respect to nuclear coordinate of the atom, at which the ϕ_γ function is centered. Introducing the shorthand notation

$$\begin{aligned} &S(\delta; i_\gamma, j_\gamma, k_\gamma, \zeta_\gamma) \\ &\quad = \int (x - X_\delta)^{i_\delta} (y - Y_\delta)^{j_\delta} (z - Z_\delta)^{k_\delta} e^{-\zeta_\delta |r - R_\delta|^2} \\ &\qquad \times (x - X_\gamma)^{i_\gamma} (y - Y_\gamma)^{j_\gamma} (z - Z_\gamma)^{k_\gamma} \\ &\qquad \times e^{-\zeta_\gamma |r - R_\gamma|^2} \, dx \, dy \, dz, \end{aligned} \tag{B–15}$$

the nonvanishing x component can be written as:

$$\begin{aligned} \left\langle \phi_\delta \left| \frac{\partial}{\partial X_\gamma} \right| \phi_\gamma \right\rangle &= -i_\gamma S(\delta; i_\gamma - 1, j_\gamma, k_\gamma, \zeta_\gamma) \\ &\quad + 2\zeta_\gamma S(\delta; i_\gamma + 1, j_\gamma, k_\gamma, \zeta_\gamma) \end{aligned} \tag{B–16}$$

and analogous equations for the y and z components hold. The AO derivative coupling integrals are thus transformed to overlap integrals over Cartesian Gaussian functions with different angular momentum, which are well known (see, e.g., Ref. [32]).

In summary, the implementation of simple analytic expressions derived for nonadiabatc couplings in the framework of the "frozen ionic bonds" approximation allows us to carry out nonadiabatic dynamics at low computational demand.

ACKNOWLEDGMENTS

This work was supported by the "Sonderforschungsbereich 450, Analyse und Steuerung photoinduzierter ultraschneller Reaktionen" of the *Deutsche Forschungsgemeinschaft*. The calculations have been partly carried out at the *Konrad-Zuse-Zentrum für Informationstechnik*, Berlin. V. Bonačić-Koutecký thanks the *Miller Institute for Basic Research in Science, University of California*, for *Visiting Miller Research Professorship*.

References

1. Zewail, A. H. Faraday Discuss Chem Soc 1991, 91, 207.
2. Mokhtari, A.; Cong, P.; Herek, J. L.; Zewail, A. H. Nature 1990, 348, 225.
3. Dantus, M.; Bowman, R. M.; Gruebele, M.; Zewail, A. H. J Chem Phys 1989, 91, 7437.
4. Weaver, A.; Metz, R. B.; Bradforth, S. E.; Neumark, D. M. J Chem Phys 1990, 93, 5352.
5. Metz, R. B.; Neumark, D. M. J Chem Phys 1992, 97, 962.
6. Neumark, D. M. Accounts Chem Res 1993, 26, 33.
7. Burnett, S. M.; Stevens, A. E.; Feigerle, C. S.; Lineberger, W. C. Chem Phys Lett 1983, 100, 124.
8. Ervin, K. M.; Ho, J.; Lineberger, W. C. J Chem Phys 1989, 91, 5974.
9. Wenthold, P. G.; Hrovat, D.; Borden, W. T.; Lineberger, W. C. Science 1996, 272, 1456.
10. Wolf, S.; Sommerer, G.; Rutz, S.; Schreiber, E.; Leisner, T.; Wöste, L.; Berry, R. S. Phys Rev Lett 1995, 74, 4177.
11. Boo, D. W.; Ozaki, Y.; Andersen, L. H.; Lineberger, W. C. J Phys Chem A 1997, 101, 6688.
12. Jortner, J. In Femtochemistry; Chergui, M., Ed.; World Scientific: Singapore, 1996.
13. Jortner, J. Z Phys D 1992, 24, 247.
14. Hartmann, M.; Pittner, J.; Bonačić-Koutecký, V.; Heidenreich, A.; Jortner, J. J Chem Phys 1998, 108, 3096.
15. Hartmann, M.; Heidenreich, A.; Pittner, J.; Bonačić-Koutecký, V.; Jortner, J. J Phys Chem A 1998, 102, 4069.
16. Jortner, J. J Chem Phys 1995, 92, 205.
17. Jortner, J.; Levine, R. D. Isr J Chem 1990, 30, 207.
18. Reichardt, D.; Bonačić-Koutecký, V.; Fantucci, P.; Jellinek, J. Z Phys D 1997, 40, 486.
19. Hartmann, M.; Pittner, J.; van Dam, H.; Bonačić-Koutecký, V. Eur Phys J D 1999, 9, 393.
20. Hartmann, M.; Pittner, J.; Bonačić-Koutecký, V. J Chem Phys 2001, 114, 2106.
21. Hartmann, M.; Pittner, J.; Bonačić-Koutecký, V. J Chem Phys 2001, 114, 2123.
22. Yarkony, D. R. Rev Modern Phys 1996, 68, 985.
23. Domcke, W.; Stock, G. Advances in Chemical Physics, Vol. 100; Prigogine, I.; Rice, S. A., Eds.; Wiley: New York, 1997.
24. Tully, J. C. J Chem Phys 1990, 93, 1061.
25. Fang, J.-Y.; Hammes-Schiffer, S. J Phys Chem A 1999, 103, 9399.
26. Hillary, M.; O'Connell, R. F.; Scully, M. O.; Wigner, E. P. Phys Rep 1984, 106, 121.
27. Bonačić-Koutecký, V.; Pittner, J.; Koutecký, J. Chem Phys 1996, 210, 313; Bonačić-Koutecký, V.; Pittner, J. Chem Phys 1997, 225, 173.
28. Pittner, J. Ab Initio Study of Optical Properties of Neutral and Charged Pure and Mixed Alkali Metal Clusters, Dissertation, Humboldt-Universität zu Berlin, Verlag für Wissenschaft und Forschung: Berlin, 1997.
29. Ochsenfeld, C.; Gauss, J.; Ahlrichs, R. J Chem Phys 1995, 103, 7401.
30. van Caillie, C.; Amos, R. Chem Phys Lett 1999, 308, 249.
31. van Dam, H.; Pittner, J.; Hartmann, M.; Bonačić-Koutecký, V., to be published.
32. Yamaguchi, Y.; Osamura, Y.; Goddard, J. D.; Schaefer, III, H. F. A New Dimension to Quantum Chemistry: Analytic Derivative Methods in Ab Initio Molecular Electronic Structure Theory; Oxford University Press: New York, 1994, p. 72, Eq. (5.26).
33. Yamaguchi, Y.; Osamura, Y.; Goddard, J. D.; Schaefer, III, H. F. A New Dimension to Quantum Chemistry: Analytic Derivative Methods in Ab Initio Molecular Electronic Structure Theory; Oxford University Press: New York, 1994, p. 148, Eq. (11.20).
34. Yamaguchi, Y.; Osamura, Y.; Goddard, J. D.; Schaefer, III, H. F. A New Dimension to Quantum Chemistry: Analytic Derivative Methods in Ab Initio Molecular Electronic Structure Theory; Oxford University Press: New York, 1994, p. 152, Eq. (11.39).
35. Rice, J. E.; Amos, R. D.; Handy, N. C.; Lee, T. J.; Schaefer, H. F. J Chem Phys 1986, 85, 963.
36. Lee, T. J.; Handy, N. C.; Rice, J. E.; Scheiner, A. C. Schaefer, H. F. J Chem Phys 1986, 85, 3930.
37. Miller, W. H. Faraday Discuss 1998, 110, 1.
38. Herman, M. F. Int J Quantum Chem 1998, 70, 897; J Chem Phys 1995, 103, 8081; J Chem Phys 1999, 110, 4141.
39. Martinez, T.; Ben-Nun, M.; Levine, R. D. J Phys Chem 1996, 100, 7884; Ben-Nun, M.; Martinez, T. J Chem Phys 1998, 108, 7244; Ben-Nun, M.; Martinez, T. J Chem Phys 1999, 110, 4134; Ben-Nun, M.; Martinez, T. J Chem Phys 2000, 112, 6113.
40. Kapral, R.; Ciccotti, G. J Chem Phys 1999, 110, 8919; Nielsen, S.; Kapral, R.; Ciccotti, G. J Chem Phys 2000, 112, 6543.
41. Martens, C. C.; Fang, J.-Y. J Chem Phys 1997, 106, 4918; Donoso, A.; Martens, C. C. J Phys Chem A 1998, 102, 4291.
42. Donoso, A.; Martens, C. C. J Phys Chem A 2000, 112, 3980.
43. Robb, M. A.; Olivucci, M.; Bernardi, F. Photochemistry, In The Encyclopedia of Computational Chemistry; Schleyer, P. V. R.; Allinger, N. L.; Clark, T.; Gasteiger, J.; Kollman, P. A.; Schaefer, III, H. F.; Schreiner, P. R., Eds.; Wiley: Chichester, 1998, pp. 2056–2064.
44. Michl, J.; Bonačić-Koutecký, V. Electronic Aspects of Organic Photochemistry; Wiley: New York, 1990.
45. Bonačić-Koutecký, V.; Köhler, J.; Michl, J. Chem Phys Lett 1984, 104, 440.
46. Bonačić-Koutecký, V.; Koutecký, J.; Michl, J. Angew Chemie Int Ed Engl 1987, 26, 170.
47. Bonačić-Koutecký, V.; Schöffel, K.; Michl, J. Theor Chim Acta 1987, 72(5–6), 459.
48. Schoenlein, R. W.; Peteanu, L. A.; Mathies, R. A.; Shank, C. V. Science 1991, 254, 412.
49. Ottolenghi, M.; Sheves, M. Isr J Chem 1995, 35.
50. See Becker, R. S. Photochem Photobiol 1988, 48, 369.